Check for updates

AGU ADVANCING EARTH AND SPACE SCIENCES

Water Resources Research

RESEARCH ARTICLE
10.1029/2024WR039276

The Impact of Climate and Land Cover Change on the Cryosphere and Hydrology of the Mackenzie River Basin, Canada

Mohamed E. Elshamy[1,2], John W. Pomeroy[1,2], Alain Pietroniro[2,3], Howard Wheater[1,4], and Mohamed Abdelhamed[1]

[1]Global Institute for Water Security, University of Saskatchewan, Saskatoon, SK, Canada, [2]Centre for Hydrology, University of Saskatchewan, Saskatoon, SK, Canada, [3]Schulich School of Engineering, University of Calgary, Calgary, AB, Canada, [4]Department of Civil and Environmental Engineering, Imperial College London, London, UK

Abstract Northern basins are projected to continue warming at rates higher than the global average, with the impacts of warming compounded by concomitant deglaciation, permafrost thaw and vegetation shifts. The Mackenzie River Basin drains headwaters in the glaciated Canadian Rockies to the Arctic Ocean and is mostly underlain by permafrost. Scenarios of future change in this basin were simulated using the MESH distributed hydrological-cryospheric land surface model. MESH was forced with bias-corrected, downscaled RCM forcings and parameterized with a deep subsurface profile, organic soils, and glaciers. The model, validated against discharge, snowpack, and permafrost observations, was used to simulate 21st century hydrology and permafrost dynamics under the RCP8.5 emissions scenario, incorporating projected land cover change applied at two discrete time steps (2021 and 2065). The findings indicate a rapid acceleration of permafrost thaw. By the 2080s, most of the basin will be devoid of permafrost. By late century, river discharges shift to earlier and higher peaks in response to projected increases in precipitation, temperature and snowmelt, despite increases in evapotranspiration from longer snow-free seasons. Baseflow discharges increase in winter, due to higher precipitation and increased basin connectivity from permafrost thaw resulting in enhanced groundwater flow. Subsurface moisture storage rises slightly but the liquid water fraction increases dramatically, increasing subsurface runoff and river discharge. Canadian Rockies' deglaciation reduces summer and annual discharge in the Athabasca and Peace headwaters. Downstream and northward of the mountain headwaters the direct impacts of climate change on river discharge dominate those of changing land cover and glaciers.

Plain Language Summary The Mackenzie River Basin, a large northern water system that stretches from the Canadian Rockies to the Arctic Ocean, is undergoing large changes due to rapid climate warming in northern latitudes. This study simulated how climate and land cover changes could impact the basin's water flows and permafrost (frozen ground for at least 2 years) using a land surface model. It is expected that climate change will bring warmer temperatures and higher precipitation over the basin. The model predicts that most permafrost areas will disappear by the 2080s. Permafrost thaw could lead to more groundwater flow and higher winter river levels as more water moves through the ground. Warmer temperatures will cause snow to melt earlier, resulting in higher river flows earlier in the year. Additionally, as glaciers in the Rockies melt, summer river flows will decrease, especially in headwater areas like the Athabasca and Peace Rivers. However, the overall effect of warmer temperatures and increased rainfall will likely be stronger than changes from shrinking glaciers and other land cover changes. These findings highlight the need for planning for and adapting to shifts in northern river systems due to climate change.

Key Points:

- Streamflow is expected to peak higher and earlier for most subbasins of the Mackenzie River Basin in response to climate change
- Most of the basin is expected to be permafrost-free by 2080s under RCP8.5 resulting in higher connectivity and larger subsurface flows
- Deglaciation of mountainous headwaters is expected to reduce summer flows with implications for water resources management and navigation

Supporting Information:

Supporting Information may be found in the online version of this article.

Correspondence to:

M. E. Elshamy,
mohamed.elshamy@usask.ca

Citation:

Elshamy, M. E., Pomeroy, J. W., Pietroniro, A., Wheater, H., & Abdelhamed, M. (2025). The impact of climate and land cover change on the cryosphere and hydrology of the Mackenzie River Basin, Canada. *Water Resources Research*, *61*, e2024WR039276. https://doi.org/10.1029/2024WR039276

Received 28 OCT 2024
Accepted 18 NOV 2025

Author Contributions:

Conceptualization: Mohamed E. Elshamy, John W. Pomeroy, Alain Pietroniro, Howard Wheater
Data curation: Mohamed E. Elshamy
Formal analysis: Mohamed E. Elshamy, Mohamed Abdelhamed
Funding acquisition: John W. Pomeroy, Howard Wheater
Methodology: Mohamed E. Elshamy, John W. Pomeroy, Alain Pietroniro, Mohamed Abdelhamed

© 2025. The Author(s).
This is an open access article under the terms of the Creative Commons Attribution-NonCommercial-NoDerivs License, which permits use and distribution in any medium, provided the original work is properly cited, the use is non-commercial and no modifications or adaptations are made.

1. Introduction

Anthropogenic climate change is evident in various aspects of the Earth's system. Notable alterations include the increase of mean and extreme annual and seasonal air temperatures, altered spatial and temporal precipitation patterns and changes in phase (snowfall vs. rainfall), changes to the frequency of compound events such as mixed phase precipitation and rain on snow events, heatwaves, and the modification of incoming solar radiation (Abdelmoaty et al., 2021; Liu et al., 2021; Quante et al., 2021; Rajulapati et al., 2022). Such changes have major implications for the hydrological cycle (DeBeer et al., 2021), biogeochemical cycles (Jansson & Hofmockel, 2020; Tittensor et al., 2021), and water resources management (Busschaert et al., 2022; Yun et al., 2021).

Project administration: John W. Pomeroy, Alain Pietroniro, Howard Wheater
Supervision: John W. Pomeroy, Alain Pietroniro, Howard Wheater
Validation: Mohamed E. Elshamy
Visualization: Mohamed E. Elshamy, Mohamed Abdelhamed
Writing – original draft: Mohamed E. Elshamy, Mohamed Abdelhamed
Writing – review & editing: Mohamed E. Elshamy, John W. Pomeroy, Alain Pietroniro, Howard Wheater, Mohamed Abdelhamed

Continental high latitudes have been warming at higher rates than the global average (DeBeer et al., 2016; Zhang et al., 2019) and this is expected to continue under all future emission scenarios (Derksen et al., 2019). Moreover, feedback loops play a pivotal role in amplifying or lessening the impact and extent of climate change (Betts et al., 1996). In arctic and subarctic regions, the release of greenhouse gases stored in the terrestrial subsurface represents a critical positive feedback that could accelerate climatic alterations (Burke et al., 2020; McGuire et al., 2018). According to Schuur et al. (2015), the carbon dioxide and methane stored in the top 3-m of permafrost exceeds by two-fold the amount currently existing in the atmosphere. The release of carbon from this massive store, along with the expected decline of snow and ice cover, could irreversibly shift the planetary system into a new state, far warmer than the target of the Paris Agreement (Schellnhuber et al., 2016).

The Mackenzie River Basin (MRB) is one of the largest drainage basins in North America, contributing over 300 km^3 flow annually into the Arctic (Rood et al., 2017). This exerts significant influence on oceanographic processes, coastal dynamics, biodiversity, and climate feedbacks, both regionally and globally (Aagaard & Carmack, 1989; Carmack et al., 2016; McPhee et al., 2009; Yang et al., 2015). The MRB covers 1.8 million km^2 (18% of Canada's area), and hosts diverse ecosystems, permafrost landscapes, and Indigenous communities. Recently, the region has experienced significant environmental change, attributed to the interplay of local and regional activities (e.g., mining) and global (e.g., climate) change. These changes have had profound impacts on hydrological regimes, land subsidence, permafrost stability, vegetation growth and succession, and wildfire occurrence (DeBeer et al., 2021; Walvoord & Kurylyk, 2016; Woo et al., 2007). Therefore, understanding these implications is paramount for devising effective adaptation and mitigation strategies in the face of these escalating global environmental challenges (Cohen, 1997; Ford et al., 2018).

Permafrost, defined as the ground that stays cryotic (i.e., temperature $\leq 0°C$) for at least two consecutive years (van Everdingen, 2005), underlays almost a quarter of the Northern Hemisphere's landmass and a considerable portion of the MRB. It is a pivotal component in cold regions, affecting hydrology, energy and water flux partitioning, carbon dynamics and plant communities (Walvoord & Kurylyk, 2016; Woo et al., 1992). Shur and Jorgenson (2007) viewed permafrost as a sensitive climate change indicator, although Zhang et al. (2008) noted the disequilibrium response of permafrost to climate warming (throughout 1850–2100) due to its long-term thermal memory. Observation-based studies have highlighted spatial changes in permafrost state in recent decades, mostly thaw and degradation in response to climate warming (Farquharson et al., 2019; Harris et al., 2009; Morse et al., 2016; Romanovsky et al., 2010; Smith et al., 2012; Zhao et al., 2010). Additionally, the heterogeneous nature of permafrost thaw alters subsurface moisture regimes, which affects the spatial hydrological connectivity of landscape features (Baltzer et al., 2014; Beilman & Robinson, 2003; Quinton et al., 2011). These changes influence streamflow and its seasonality, particularly increasing winter flows (Connon et al., 2014), and impact the partitioning of water storage above and below ground (Woo, 2012).

Over decadal to century time scales, vegetation is expected to adapt to changes in precipitation, temperature, snow cover, permafrost, and subsurface moisture. While some systematic changes in vegetation types are likely, the greatest impacts of climate change on vegetation dynamics are expected to occur indirectly, primarily through increased frequency and intensity of disturbances (e.g., wildfire, insect outbreaks) (Turetsky et al., 2017) which have already become more common across the Boreal Forest in recent decades (Hanes et al., 2019). Expected changes include the expansion of shrubs northwards, replacing barren or tundra grasslands, and advancing Northern and Alpine tree lines (DeBeer et al., 2021). Forest cover may also change in response to wildfire and other disturbances (e.g., pests and insects), resulting in complex patterns of tree species replacements (e.g., broadleaf trees replacing needleleaf ones) (Johnstone et al., 2010). Warming may also favor agricultural expansion in some northern forested or grassland landscapes (Agyeman et al., 2023), leading to further forest clearing and feedback to climate change (Hannah et al., 2020). One of the most certain land cover changes is the ongoing and accelerating glacier shrinkage or disappearance (Clarke et al., 2015; Rounce et al., 2023; Shannon et al., 2019), affecting streamflow from glaciated headwaters, especially in late summer.

Numerical models are valuable tools for simulating and predicting the coevolution of hydrology and permafrost. Given the interdependency between energy and water fluxes and stores within permafrost (Riseborough et al., 2008; Walvoord & Kurylyk, 2016), Earth System Models (ESMs) and their land-surface components (Land Surface Models: LSMs) have been continually enhanced to better simulate thermo-hydrological processes in permafrost regions (Alexeev et al., 2007; Ji et al., 2022; Lawrence et al., 2008) and project its evolution under global warming (Burke et al., 2020; Lawrence & Slater, 2008). However, ESM-based projections encompass

19447973, 2025, 12, Downloaded from https://agupubs.onlinelibrary.wiley.com/doi/10.1029/2024WR039276 by University Of Saskatchewan, Wiley Online Library on [08/12/2025]. See the Terms and Conditions (https://onlinelibrary.wiley.com/terms-and-conditions) on Wiley Online Library for rules of use; OA articles are governed by the applicable Creative Commons License

19447973, 2025, 12, Downloaded from https://agupubs.onlinelibrary.wiley.com/doi/10.1029/2024WR039276 by University Of Saskatchewan, Wiley Online Library on [08/12/2025]. See the Terms and Conditions (https://onlinelibrary.wiley.com/terms-and-conditions) on Wiley Online Library for rules of use; OA articles are governed by the applicable Creative Commons License

various uncertainties, including model structural uncertainty, climate scenario uncertainty, and internal climate variability (Deser et al., 2012; Gao et al., 2020), which collectively introduce significant bias into the analysis of permafrost evolution (Burke et al., 2020). Additionally, the paucity of permafrost observations limits the validation of these models, as available data are too sparse to capture the spatial heterogeneity of permafrost and its thaw (Lamontagne-Hallé et al., 2020; Pastick et al., 2014). Despite significant effort towards mapping permafrost over large domains (e.g., Aalto et al., 2018; Chadburn et al., 2017; Gruber, 2012; Obu et al., 2019; Ran et al., 2022) and given that permafrost cannot be directly detected via current remote sensing technology (Westermann et al., 2015), the scarcity of ground truth data remains unresolvable.

The MRB has been the focus of many regional and global hydrology and climate research projects and programmes, including the **MA**ckenzie **G**EWEX **S**tudy (MAGS) (Pietroniro & Soulis, 2003; Stewart et al., 1998; Woo, 2008a, 2008b). MAGS significantly advanced the understanding of key cold region hydrological processes and contributed to the development of the WATCLASS modelling framework (Soulis et al., 2000; Soulis & Seglenieks, 2008), which improved hydrological representation within the Canadian Land Surface Scheme (Verseghy, 1991; Verseghy et al., 1993). This work later evolved into the MESH modelling framework, which is used in this study.

Within MAGS, several attempts to close the water balance of the MRB for specific years were conducted (Louie et al., 2002; Strong et al., 2002) utilizing field data and various remotely sensed data sets. Yip et al. (2012) used the WATFLOOD (Kouwen, 1988) distributed hydrological model at 20 km spatial resolution run at a daily time step to examine the trends of hydrological variables over a 40-year historical period (1961–2002). These studies highlighted the importance of coupling the energy and water balances to properly simulate cold region processes such as snow accumulation, redistribution and melt (Pomeroy et al., 2008), and seasonal and permanent frozen soil dynamics (Woo & Marsh, 2005). MAGS also examined the maximum active layer at a few locations in the Mackenzie Valley using probabilistic approaches (Woo et al., 2007).

Building on these foundational studies, research on the Canadian Arctic Basins, including the MRB, has extensively used various modeling approaches to investigate long-term changes in streamflow. Burn (2008) identified significant upward trends in streamflow and earlier spring freshet timings linked to increasing temperatures from 1947 to 2005 through time-series analysis. Further extending this analysis, Jacques and Sauchyn (2009) and Rood et al. (2017) found similar trends from 1939 to 2007 and 1913–2005, respectively. Early catchment-scale models like SLURP (Thorne, 2011) and SLURP and Mac-PDM.09 (Gosling et al., 2011) projected increases in low and high flows with earlier seasonal peaks, though results varied by climate model. Similarly, Gelfan et al. (2017) and Shrestha et al. (2019) predicted gradual increases in flow and earlier peaks due to earlier snowmelt using semi-distributed models (ECOMAG, HYPE, and VIC). Teufel and Sushama (2019) employed Regional Climate Models (RCMs) and Earth System Models (ESMs) and projected abrupt changes and a shift from high to low-flow conditions, though these projections were questioned due to model assumptions and data (O'Neill et al., 2020). Zhang et al. (2023) applied several machine-learning approaches that forecast increased winter flows, significantly contributing to average streamflow increases. Using MESH, Rokaya et al. (2019b) found earlier and higher streamflow peaks in the Smoky River, a tributary of the Peace River, in response to climate change. Collectively, these studies highlight trends towards increasing streamflow and earlier peaks due to climate change, with variations depending on modeling frameworks.

Despite these advances, regional and global hydrological models have often relied on conceptual approaches derived from catchment-scale models, typically using coarse spatial and temporal resolutions, and not explicitly solving the energy balance or properly simulating permafrost dynamics via a deep-enough subsurface profile. Attempts using LSMs (e.g., Abdelhamed et al., 2024; Rokaya et al., 2019b) were limited to a few subbasins of the MRB. To address these gaps, Elshamy et al. (2025) developed a high fidelity cryo-hydrological model of the entire MRB using the MESH framework, validated extensively against streamflow, snowpack, ET, and permafrost in situ and remote sensing data sets. This study leverages this model to project the impacts of climate and land cover and use changes on the basin's hydrology and permafrost, exploring the linkages between surface and subsurface changes. The study evaluates, for example, how the water balance components change over time under climate and land cover changes, how total precipitation is partitioned between runoff and evapotranspiration, whether there are important shifts in runoff regimes in terms of runoff composition and how that is affected by glacier retreat and permafrost thaw.

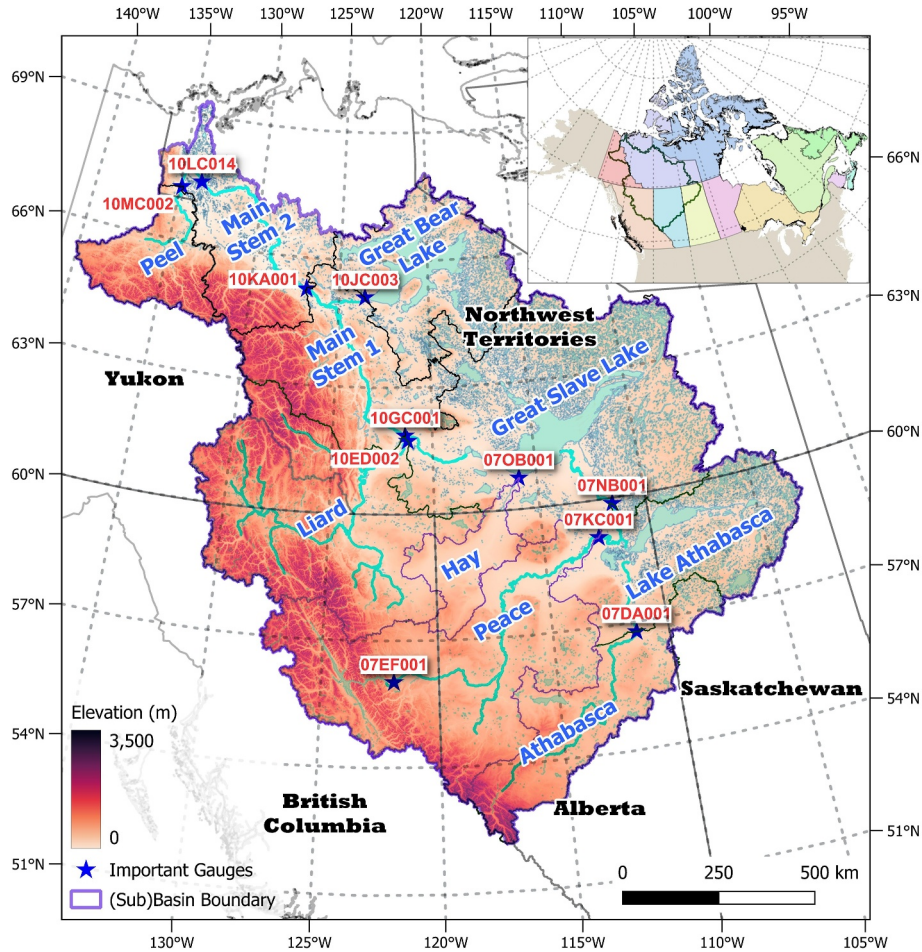


Figure 1. Mackenzie River Basin: Location (indicated by the inset), elevations, Provinces and Territories (black labels and borders) and main subbasins (blue labels) with Water Survey Canada (WSC) gauge IDs of their outlets (red labels).

The paper is organized as follows: Section 2 presents the study area and the model, Section 3 describes the future change scenarios used to force the model, Section 4 discusses future projections for hydrological fluxes, water balance, glacier contributions and permafrost, and Section 5 provides further discussions, conclusions, and recommendations. Sections, Tables, and Figures denoted "S" refer to the Supporting Information S1.

2. Model and Data Sets

2.1. Study Area

The 1.8 million km^2 Mackenzie River Basin (MRB) (Figure 1) drains much of western and northwestern Canada, including parts of the provinces of Saskatchewan, Alberta, and British Columbia, as well as the Yukon Territory and the Northwest Territories (Natural Resources Canada, 2006). As noted above, the average annual discharge of more than 300 km^3 to the Arctic Ocean via the Beaufort Sea influences regional and global oceanic and atmospheric circulations, hence changing discharge patterns have potential implications for future climate.

The diverse climate, hydrology, and ecology of the basin, together with its large scale, present significant challenges for modelling. The mountainous headwaters of the Athabasca, Peace, and Liard rivers (the western tributaries) include Canada's largest interior icefields (e.g., Columbia and Britnell-Bologna), have year-round snow-cover, and are characterized by steep slopes and high discharges, primarily due to snow and glacier melt. In contrast, the eastern tributaries, located on the Canadian Shield, are characterized by thousands of interconnected lakes and swamps. The three largest lakes, the Athabasca, the Great Slave, and the Great Bear, have a combined area of 67,576 km^2 (Natural Resources Canada, 2006), and thus represent major controls on the

19447973, 2025, 12, Downloaded from https://agupubs.onlinelibrary.wiley.com/doi/10.1029/2024WR039276 by University Of Saskatchewan, Wiley Online Library on [08/12/2025]. See the Terms and Conditions (https://onlinelibrary.wiley.com/terms-and-conditions) on Wiley Online Library for rules of use; OA articles are governed by the applicable Creative Commons License

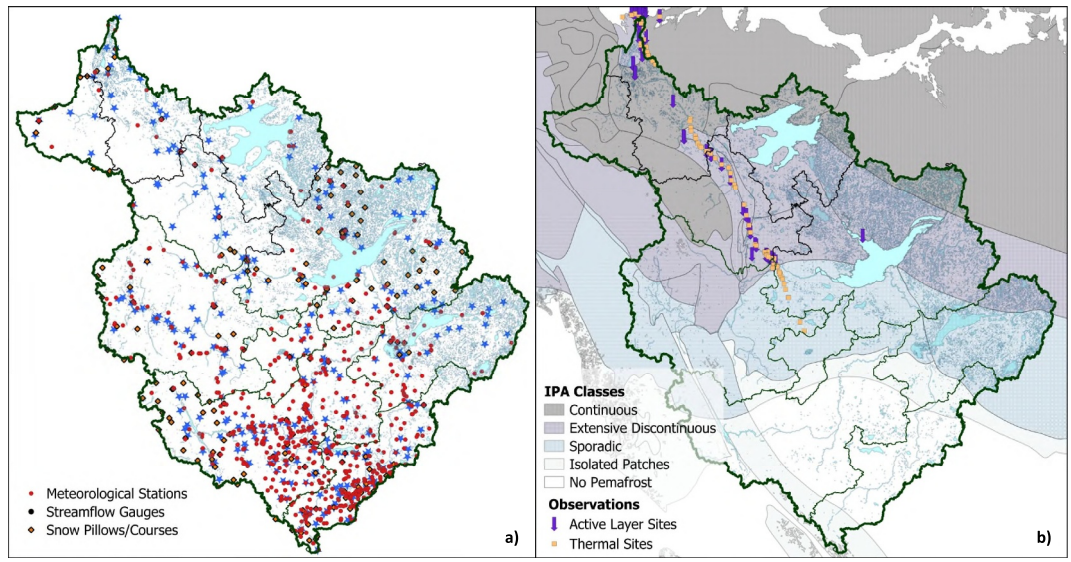


Figure 2. (a) Locations of Meteorological Survey Canada (MSC) stations, Water Survey Canada (WSC) streamflow gauges and snow pillows and courses from CanSWE v5 (Vionnet et al., 2021) within the MRB, and (b) Permafrost Zones underlying the MRB according to the International Permafrost Association (IPA) classification and locations of observational sites within the basin extracted from Geological Survey Canada (GSC) reports.

river's flow regime. The basin also includes three important deltas: the Peace-Athabasca, Slave River, and Mackenzie Delta (at its outlet to the Arctic Ocean). Despite the scale and diversity of the basin, observations are sparse in terms of streamflow, snow and meteorology (Figure 2a), especially in the more remote areas to the North and East.

According to the circumpolar permafrost map of the International Association of Permafrost (IPA) (Brown et al., 2002; Figure 2b), about 75% of the basin is underlain by either continuous (in its northern part), discontinuous (to the south of the continuous region), or sporadic or patchy permafrost (in the southern parts of the Liard, in the Hay subbasin, and the Rocky Mountains). However, in situ permafrost observations, which are primarily available from sites established to monitor permafrost conditions for infrastructure, for example the Norman Wells-Zama oil pipeline and the Mackenzie Highway, are highly concentrated along the Mackenzie Valley and Delta (Figure 2b).

2.2. The MESH Modelling Framework

MESH typically uses a regular latitude-longitude grid and couples a semi-distributed land surface model (LSM) with streamflow routing (Pietroniro et al., 2007; Wheater et al., 2022). It has been widely used in Canada at a variety of scales; large scale applications include the Saskatchewan River Basin (Yassin et al., 2017) and the Great Lakes basins (Mai et al., 2021). The LSM simulates vertical heat and moisture flux transfers between land surface and atmosphere using either the Canadian Land Surface Scheme (CLASS: Verseghy, 2012), as used here, or the Soil, Vegetation and Snow scheme (SVS: Husain et al., 2016). Unlike many LSMs, MESH incorporates a sloped vertical column to allow lateral transfers of runoff, both as overland or surface flow and as interflow or subsurface flow (Soulis et al., 2000) to an assumed stream within each model grid cell. Inter-grid flow routing is based on the WATROUTE algorithm from the WATFLOOD distributed hydrological model (Kouwen, 1988). For computational efficiency, sub-grid heterogeneity is represented using the grouped response unit (GRU) approach, whereby different units within a grid cell do not have specific locations or interact explicitly (Kouwen et al., 1993). A GRU is typically defined by a land cover class, but other factors can be included, such as soil type, slope, and aspect. Recent MESH developments include improved representation of baseflow (Luo et al., 2012), controlled reservoirs (Yassin et al., 2019) and permafrost (Elshamy et al., 2020). MESH has been coupled to other models, for example the river ice model of Rokaya et al. (2019a) to examine the impacts of climate change and regulation on ice jam flooding of the Peace River, a major tributary of the MRB. MESH's history and developments are described further in Wheater et al. (2022).

19447973, 2025, 12, Downloaded from https://agupubs.onlinelibrary.wiley.com/doi/10.1029/2024WR039276 by University Of Saskatchewan, Wiley Online Library on [08/12/2025]. See the Terms and Conditions (https://onlinelibrary.wiley.com/terms-and-conditions) on Wiley Online Library for rules of use; OA articles are governed by the applicable Creative Commons License

2.3. The MRB MESH Model

The model configuration for the MRB involved extensive use of diverse data sets to accurately define the basin's physiographic and hydrological characteristics. Key data sets included the Canadian Digital Elevation Model (CDEM) (Natural Resources Canada, 2013) and the 2005 North American Land Cover data set (Canada Centre for Remote Sensing (CCRS) et al., 2010). The CDEM (resampled to 150 m resolution from $0.75'' \times 0.75'' - 1.5''$) was used to develop a drainage database encompassing basin boundary, flow directions, channel lengths, and internal grid slopes, aligning closely with Water Survey Canada (WSC) reported values to ensure that the modelled streamflow matched observed data. The resolution of the MESH model was selected as $0.125° \times 0.125°$ (~10 km on average), to match the forcing and as a compromise between accuracy and computational demands.

The 2005 North American Land Cover data set provided land cover classifications based on MODIS images (250 m resolution), consolidated into 11 classes (from an original 19) to balance computational efficiency and parameterization needs. This classification was crucial for representing the predominant Boreal Forest, water bodies, and wetlands within the MRB. Potential vegetation shifts due to climate change, such as the replacement of tundra by shrubs or the northward advancement of the treeline, were considered to enable the simulation of possible future changes in land cover (Section 3.2) and their hydrological impacts. The model also accounted for significant features like glaciers (Section 3.3), which, despite their small area, substantially impact headwater hydrology.

An important consideration when building the MRB model (see Elshamy et al., 2025 for model configuration and validation details) was to address the representation of permafrost, given the current degradation trends and their major impact on landforms and hydrological connectivity, and thus on the basin's hydrology. Hence, a deep subsurface profile was used to simulate permafrost dynamics, careful attention was paid to model initialization, and the model was validated against various permafrost observations. The subsurface profile was configured with 25 layers extending to a depth of 51.24 m (Elshamy et al., 2020), with fine discretization in the top 2 m where the active layer depth is typically located. Special attention was also given to organic soils and the hydrologically active soil depth, or depth to bedrock (SDEP), which significantly impact water and energy balance components and permafrost insulation. The Soil Landscapes of Canada (SLC) version 2.2 (Centre for Land and Biological Resources Research, 1996) provided soil texture data (percentages of sand, clay, and organic matter) needed to estimate spatially varying hydraulic and thermal properties crucial for water and heat fluxes through the subsurface layers. SDEP was spatially varied using the Shangguan et al. (2017) data set while the organic content was used to vary the number of organic layers (Elshamy et al., 2025), allowing for improved permafrost simulations.

Incorporating lakes and reservoirs was necessary despite the added complexity. Many in the MRB are extremely large, and these water bodies play a critical role in modulating streamflow and serving as storage components. The model explicitly included 23 natural lakes and one managed reservoir, parameterizing their storage and outflow characteristics using data from WSC and other studies. Lakes were represented by their storage volume and outflow characteristics, while the Williston Reservoir was modelled by incorporating management rules for water release based on operational guidelines (Yassin et al., 2019).

At least 6-hourly climate forcing data is required for the model's energy and water balance calculations, including air temperature, total precipitation, downward shortwave and longwave radiation, surface pressure, specific humidity, and wind speed, obtained from multiple regional and global data sets. The GEM-CaPA (Côté, Desmarais, et al., 1998; Côté, Gravel, et al., 1998; Mahfouf et al., 2007; Yeh et al., 2002) reanalysis data set provided high-resolution inputs for model hydrological calibration, addressing challenges posed by the sparse and uneven distribution of meteorological stations (Figure 2a). The CanRCM4-WGC ensemble (Asong et al., 2020) was used to initialize the deep subsurface profile and evaluate model performance for permafrost utilizing data from 1951 to 2016 (see Section 3.1 for more detail regarding climate forcing). Both data sets were used at a 3-hourly time step.

Initialization focused on the thermal state of permafrost, which was validated against subsurface temperature profiles and active layer depth from point observations as well as permafrost occurrence from various spatial data sets (e.g., Aalto et al., 2018; Chadburn et al., 2017; Gruber, 2012; Obu et al., 2019; Ran et al., 2022). Special attention was given to snow cover validation, critical in the MRB due to its impact on both permafrost and runoff, where SWE data from satellite observations and ground measurements were used.

19447973, 2025, 12, Downloaded from https://agupubs.onlinelibrary.wiley.com/doi/10.1029/2024WR039276 by University Of Saskatchewan, Wiley Online Library on [08/12/2025]. See the Terms and Conditions (https://onlinelibrary.wiley.com/terms-and-conditions) on Wiley Online Library for rules of use; OA articles are governed by the applicable Creative Commons License

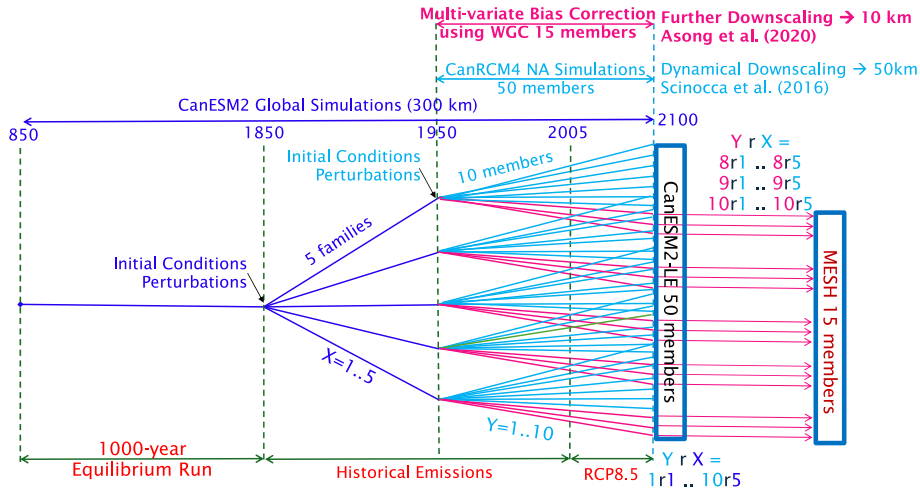


Figure 3. Construction of Climate Change Scenarios; modified after Leduc et al. (2019). *X* is the index of the ESM simulation and ranges between 1 and 5. *Y* is the index of RCM simulation (downscaling each member of *X*) and goes from 1 to 10, resulting in 50 combinations named *Y r X* which goes from 1 *r* 1 to 10 *r* 5. Downscaled members 8, 9, and 10 for all ESM families ($X = 1$ to 5) were bias-corrected and used to force MESH simulations.

Overall, the comprehensive configuration of the MESH model, integrating high-resolution land cover, topographic, soil, and climate data, allowed for effective simulation of the MRB's complex hydrology. This robust setup is believed to provide reliable insights into the basin's response to varying climatic and environmental conditions, facilitating better water resource management and planning strategies for the region. For further details on model development, configuration, and validation, please refer to Elshamy et al. (2025).

3. Future Scenarios

3.1. Climate Change

The historical and future hydrological conditions of the MRB were simulated using the CanRCM4-WGC ensemble. This comprised 15 members of the Canadian Regional Climate model version 4 (CanRCM4) simulations, bias corrected using the WFDEI-GEM-CaPA (WGC) data set (Asong et al., 2020). The CanRCM4 simulations were created by dynamically downscaling Canadian Earth System version 2 (CanESM2) simulations at 0.44° (~50 km) over the period 1950–2100 for the North American domain with 10 initial condition perturbations in 1950 for each CanESM2 member. The model, forcings, variable names, and file formats follow those used in the Coordinated Regional Downscaling Experiment (CORDEX: Giorgi et al., 2009). Following the Coupled Model Intercomparison Project Phase 5 (CMIP5) protocols (Arora et al., 2011), CanESM2 was forced by historical emissions from 1850 to 2005 and by RCP 8.5 from 2006 to 2100 (Scinocca et al., 2016) with initial conditions perturbed in 1850 to create a 5-member ensemble. Thus, the CanRCM4 simulations comprise a large ensemble of 50 members (The Canadian Regional Climate Model Large Ensemble—Open Government Portal (https://open.canada.ca/data/en/dataset/83aa1b18-6616-405e-9bce-af7ef8c2031c); Figure 3). Due to computational constraints, only 15 members of this ensemble were selected for bias correction. The 15 members were selected to encompass most of the uncertainty across the 50-member ensemble.

To remove biases in the CanRCM4 model outputs and to make them as compatible as possible with the GEM-CaPA data set used for model calibration and validation (Elshamy et al., 2025), the WFDEI-GEM-CaPA (WGC) data set was used (Asong et al., 2020). GEM-CaPA is an Environment and Climate Change Canada combined operational product from the hourly Regional Deterministic Prediction System (RDPS) forecasts produced by the Global Multiscale Model (GEM: Côté, Desmarais, et al., 1998; Côté, Gravel, et al., 1998; Yeh et al., 2002) at 10 km spatial resolution where precipitation is replaced by the Canadian Precipitation Analysis (CaPA: Fortin et al., 2018; Mahfouf et al., 2007) which assimilates observations from various sources including gauges and radar onto GEM's background field at 6 hourly time steps. CaPA is regarded as one of the best gridded precipitation products for Canada (Boluwade et al., 2018). However, the data are available only for a

19447973, 2025, 12, Downloaded from https://agupubs.onlinelibrary.wiley.com/doi/10.1029/2024WR039276 by University Of Saskatchewan, Wiley Online Library on [08/12/2025]. See the Terms and Conditions (https://onlinelibrary.wiley.com/terms-and-conditions) on Wiley Online Library for rules of use; OA articles are governed by the applicable Creative Commons License

19447973, 2025, 12, Downloaded from https://agupubs.onlinelibrary.wiley.com/doi/10.1029/2024WR039276 by University Of Saskatchewan, Wiley Online Library on [08/12/2025]. See the Terms and Conditions (https://onlinelibrary.wiley.com/terms-and-conditions) on Wiley Online Library for rules of use; OA articles are governed by the applicable Creative Commons License

comparatively short time-period, that is, since 2002 to present. The WATCH Forcing Data ERA Interim (WFDEI: Weedon et al., 2014) data set has a longer historical record (1979–2016) but a coarser resolution (0.5°). Wong et al. (2017) reported that it performed best for Canada in comparison to other long record gridded products that were assessed. WEFDEI-GEM-CaPA (WGC) is a merger of WFDEI (1979–2016) and GEM-CaPA (2005–2016) data sets to create a reference data set over the period 1979–2016 that combines the strengths of the two data sets (10 km spatial resolution and long-time span) to bias correct CanRCM4 output. Bias correction was conducted using multi-variate quantile-quantile mapping (Cannon, 2018) to produce the CanRCM4-WFDEI-GEM-CaPA (CanRCM4-WGC) data set with 0.125° (spatial) and 3-hourly (temporal) resolutions, comprised of the seven variables required by MESH. See Asong et al. (2020) for further details and evaluation of both data sets for the MRB.

Figure 4 shows the expected range of changes to the main driving climatic variables at the annual and seasonal scales from the CanRCM4-WGC ensemble (RCP 8.5). It also shows observations from the WGC data set for comparison, illustrating the quality of bias correction as WGC falls usually within the uncertainty band of CanRCM4-WGC for the period used for fitting the bias correction algorithm (1979–2008) and for the later short period (2009–2016) with few exceptions—see Section S2 in Supporting Information S1 for more discussion. In general, precipitation is expected to increase gradually by about 30% at the basin scale by 2100 (Figure 4a) mostly in autumn and spring (Figure 4b). By 2100, temperature is expected to rise by about 6.5°C (Figure 4c) with the largest increase during winter (Figure 4d). Connected to temperature, specific humidity is expected to rise as well as incoming longwave radiation (Figures 4e and 4j). There is a small downward trend in incoming shortwave radiation (Figure 4g) due to reductions mostly in spring (Figure 4h), likely due to increased cloudiness associated with increased spring precipitation. Trends in surface pressure and wind speed (Figure S2 in Supporting Information S1) are insignificant. The changes shown above are averages over the basin and thus hide some regional changes. For example, the increase in temperature is greater to the north (due to polar amplification) and east (due to lower elevations compared to the west) (Figure S3 in Supporting Information S1) while precipitation increases more in the western side of the basin (where mountains are located) compared to the east (Figure S4 in Supporting Information S1).

3.2. Vegetation Change

As climate changes, vegetation responds and interacts with those changes at long time scales spanning decades, centuries or longer to reach some form of dynamic equilibrium (Jin et al., 2023; Prentice, 1992). There are complex feedback loops between the climate and vegetation, while other elements of the Earth's system (e.g., soils, biota) also interact with vegetation and climate changes and constrain them to some extent. Some vegetation types are more resilient than others to changing climate conditions, depending on their response to disturbance such as insect outbreaks (Berg et al., 2006) and wildfire (Johnstone et al., 2010). Dynamic vegetation models exist in some land surface models, for example, CLASS-CTEM (Melton & Arora, 2016) and JULES (Best et al., 2011; Clark et al., 2011) and rely on the competition amongst different plant species to provide the dynamic vegetation properties. However, these models rarely integrate the effect of disturbances like wildfire, disease and insects that in many cases trigger the change in vegetation types. For example, a burnt needleleaf forest stand can recover post-fire into a younger needleleaf stand, or transform into shrubs or a deciduous forest, depending on a variety of conditions prior, during and post fire (Johnstone et al., 2010).

In this study, a simpler but comprehensive approach has been developed to create a future land cover change scenario, compatible with the RCP8.5 emission scenario that considers climate change only (Rehfeldt et al., 2012), constrained by expert knowledge to include additional limitations on vegetation migration. The approach is similar to that used for small cold climate mountain basins by Rasouli et al. (2019) and tied the changes to the original land cover map used for the MRB MESH model development (Elshamy et al., 2025) with integrated wildfire disturbance as a trigger, eliminating implausible changes over the modelling time frame (up to 2100). It also considered the possible expansion of agriculture into the North in response to the more favourable conditions that warming might bring such as a longer frost-free season and higher accumulation of heat units (Agyeman et al., 2021, 2023). The changes are considerable for broadleaf-mixedwood and needleleaf forests, grassland, shrubs, tundra (Lichen-Moss), croplands, and barren land cover types (Figure 5).

This leaves four of the MESH land cover types (wetlands, water bodies, glaciers, and urban) unchanged. Although deglaciation can give way to moraine lakes, the extents of other water bodies are unlikely to change significantly.

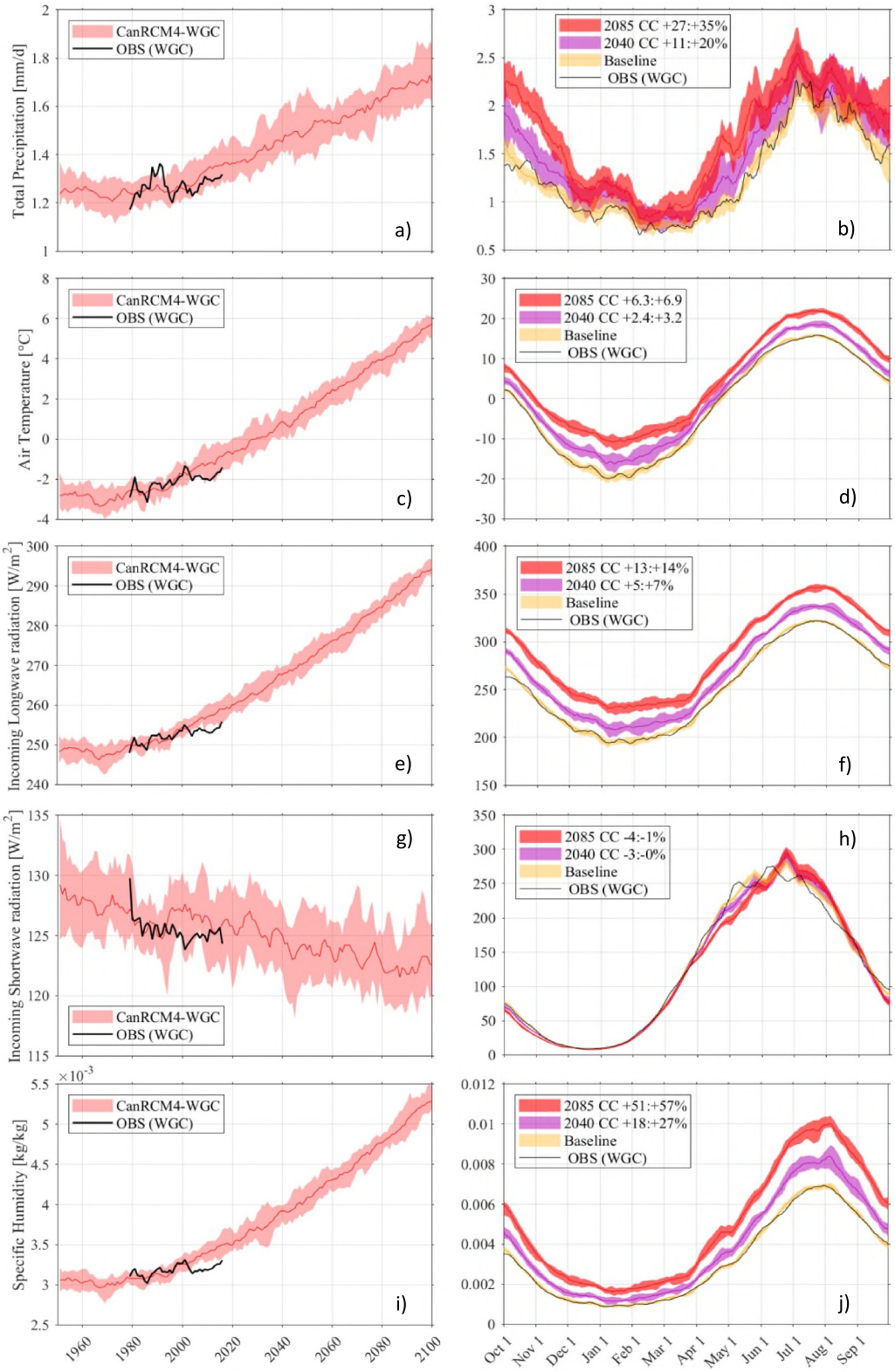


Figure 4.

19447973, 2025, 12, Downloaded from https://agupubs.onlinelibrary.wiley.com/doi/10.1029/2024WR039276 by University Of Saskatchewan, Wiley Online Library on [08/12/2025]. See the Terms and Conditions (https://onlinelibrary.wiley.com/terms-and-conditions) on Wiley Online Library for rules of use; OA articles are governed by the applicable Creative Commons License

19447973, 2025, 12, Downloaded from https://agupubs.onlinelibrary.wiley.com/doi/10.1029/2024WR039276 by University Of Saskatchewan, Wiley Online Library on [08/12/2025]. See the Terms and Conditions (https://onlinelibrary.wiley.com/terms-and-conditions) on Wiley Online Library for rules of use; OA articles are governed by the applicable Creative Commons License

The expansion of urban areas is likely but the impact of possible urbanization on the water cycle of the MRB or its tributaries is negligible as they are less than 0.01% of the basin area. Changes to wetlands are possible, as observed due to permafrost degradation in the southern sporadic and discontinuous zones, for example around the Liard River mouth (Quinton et al., 2019), but were not considered due to their highly localized and uncertain nature. Glacier retreat was integrated into the land cover change scenario as described in the next section. More details about the construction of the vegetation change scenario are provided in Appendix A of DeBeer et al. (2021). Changes to the land cover fractions summarized for the whole MRB are shown in Figure 6, segregated by region as used in the model configuration. Noticeable is the reduction in Broad Leaf Forest (BLF) in the SW part of the basin (mostly cleared for use as croplands) while it increases elsewhere. Figure S5 in Supporting Information S1 shows the changes for the remaining land cover types: grass, barren, and glaciers as in Figure 5.

Land cover changes, including glacier retreat, were introduced by changing the GRU (landcover) fractions in 2021 and 2065. Initial conditions from the CC (Climate Change) simulation on 1 Jan 2021, were used to start the LCC (Land cover and Climate Change) simulations. Although the changes were calculated progressively along the three time slices, they were introduced abruptly. Thus, a 5-year simulation period before the near future (2026–2055) and far future (2071–2100) analysis periods was used to allow the system to absorb the changes. Figure S1 in Supporting Information S1 shows the simulation timeline.

3.3. Glacier Retreat

Glacier mass loss has been widely reported in Canada and globally over recent decades and is expected to accelerate in future (DeBeer et al., 2020). Glacier ice responds directly to climate warming by losing mass but there are also indirect warming-induced feedbacks to glacier albedo related to changes in snowfall, snow cover duration, and wildfire (Aubry-Wake et al., 2022) that tend to accelerate ice melt. Glacier cover extents are likely to be reduced but this depends on a multitude of factors including the area-elevation distribution of ice in individual glaciers, redistribution of snow to glaciers and ice dynamics (Pradhananga & Pomeroy, 2022).

Clarke et al. (2015) simulated the impact of RCP 2.6, 4.5, and 8.5 on glacier ice volumes in Western Canada and the US up to 60°N, forcing their ice ablation and dynamics model by climate inputs from six Earth System Models. Projections of future glacier change for this study were taken from Clarke et al. (2015) for RCP 8.5 conducted with CanESM2 as the most compatible with the climate scenarios used here. The data set provided ice thickness time series at 200 m resolution from 2009 to 2100. To convert ice thickness to glacier fractions at the 10 km resolution of the MRB MESH model, a threshold thickness of 0.25 m was applied at the original resolution of the data set below which ice was assumed to no longer exist. Annual glacier fractions were calculated for each model grid cell, then the means over two future 30-year time slices, centred around 2040 and 2085, representing the near and far future were used. The baseline (2009) fractions from Clarke et al. (2015) CanESM2-RCP8.5 data set were slightly different from the baseline used within the model, which was corrected to Randolph Glacier Inventory v6 (RGI Consortium, 2017)—see Elshamy et al. (2025) for details. Therefore, changes between the 2040, 2085 future projections, and Clarke et al. (2015) baseline were added to the model baseline (i.e., RGIv6) to calculate the future glacier fractions. For the few grid cells in the Mackenzie mountains above 60°N that contained glaciers, the mean changes from all other grid cells were used, as these regions were not included in Clarke et al. (2015) projections. According to RGI v6.0 data, the current glaciated area in the MRB is about 1,268 km^2 (only 0.07% of the MRB area) which retreats to 513 and 64 km^2, that is only 41% and 5% remain, by 2040 and 2085 respectively. Section S4 in Supporting Information S1 includes further details.

Any change to glacier fractions (mostly reduction) is reflected as a change in the opposite direction (i.e., mostly increase) to the barren fraction of the same grid cell, that is, glaciers are assumed to be replaced by barren land. Depressional storage in barren land was not changed in the model, though proglacial lakes often form during deglaciation and can have an important local impact on post-glacial hydrology (Aubry-Wake & Pomeroy, 2023).

Figure 4. Projected changes for the main climatic forcing variables from the CanRCM4-WGC ensemble averaged over the MRB. Left panels show the mean annual time series (smoothed by a 5-year filter) and right ones show seasonal distributions for the baseline (1981–2010), near future (2026–2055) and far future (2071–2100) (smoothed by a 10-day filter) with the range of mean annual changes across the ensemble (min:max) indicated in the legend. Bands indicate the uncertainty range across the ensemble. Black lines show the WFDEI-GEM-CaPA (WGC) observational data set. Top to bottom: precipitation, air temperature, incoming longwave and shortwave radiation, and specific humidity.

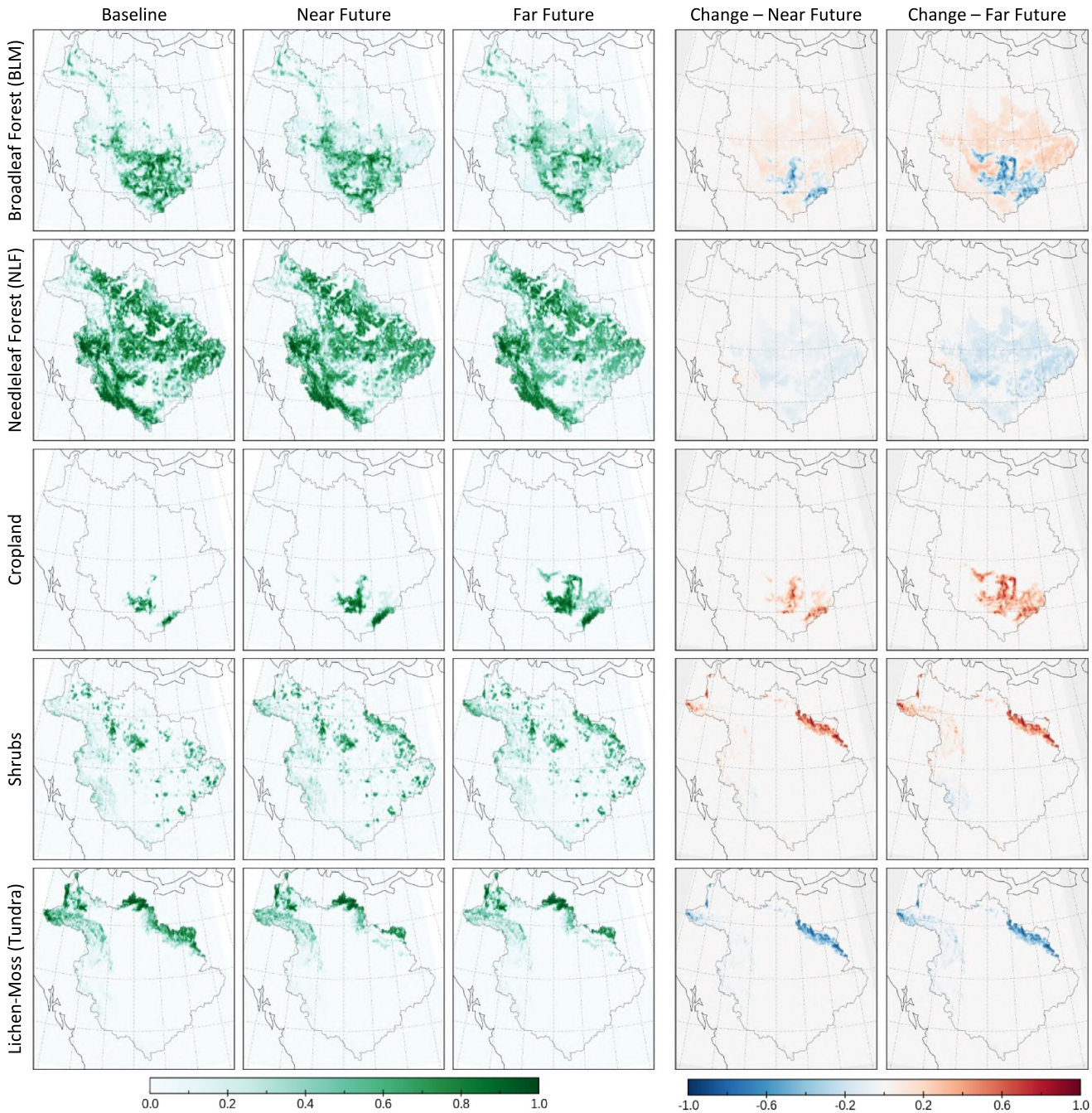


Figure 5. Land Cover Fractions [−] for the Baseline (1981–2010), Near Future (2026–2055), and Far Future (2071–2100) (left panels) and differences [−] for Near and Far Future periods from Baseline (right panels); GRUs with significant changes are shown.

4. Projected Changes

4.1. Streamflow

For most stations, there are increases in total flow volumes and higher and earlier peaks under climate change (CC) (Figure 7). Changes progressively increase over time but remain mostly within 13%–32% and 12%–36% for volume and peak flow changes, respectively in 2040, increasing to 26%–56% and 16%–60% for volume and peak flow in 2085. There are several outliers, mostly on the high side, related mostly to the subbasin size drained by those stations; smaller subbasins are likely to show exaggerated changes. The change in timing is mostly negative,

19447973, 2025, 12, Downloaded from https://agupubs.onlinelibrary.wiley.com/doi/10.1029/2024WR039276 by University Of Saskatchewan, Wiley Online Library on [08/12/2025]. See the Terms and Conditions (https://onlinelibrary.wiley.com/terms-and-conditions) on Wiley Online Library for rules of use; OA articles are governed by the applicable Creative Commons License

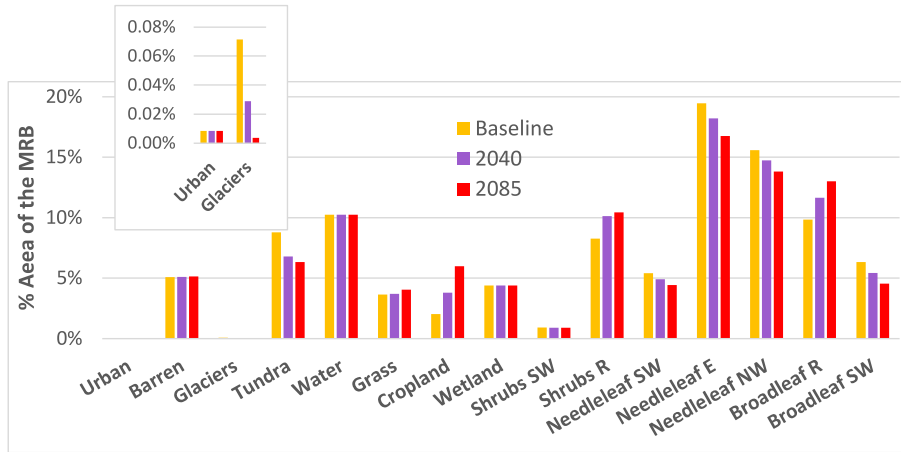


Figure 6. Changes to the overall GRU fraction [−] over the MRB for each land cover type, segregated by region when applicable (SW, E, NW, and R denote Southwest, East, Northwest, and Remainder respectively). The inset zooms onto Urban and Glacier fractions which are too small for the scale of the other GRUs.

i.e. earlier peaks by 3–11 days for 2040 and 12–24 days for 2085 are to be expected, apart from few stations located at the outlets of lakes or reservoirs where peaks are expected to occur later in the future (e.g., the highest outlier for peak time change occurs at station 07EF001, the outlet of the managed Williston Reservoir). The above quoted ranges for volume, peak flow and peak time are for the bulk of stations (25% and 75% quantiles) for the ensemble mean, and there are, of course, larger changes, and large uncertainty across the ensemble (see Figure 8 for selected stations). The additional impact of LCC shows mostly as an increase in box plot height and the number of outlier stations for all three metrics shown. The peak value and timing changes shown on Figures 7b, 7c are the ensemble mean changes calculated from the 30-year daily climatologies for the three time slices considered, calculated for each ensemble member separately before the ensemble mean shown is computed.

Changes to the seasonal flow regimes at selected key locations (Figure 8) emphasize the same trends, that is earlier and higher peaks, and larger flow volumes. The increase in flow volume is expected because precipitation increases (Figure 4a). Earlier and higher peaks result from earlier snowmelt combined with increases in spring precipitation, which is predicted to fall mostly as rain. Nevertheless, lower flows in summer are expected as rainfall increases are modest and higher temperatures (Figure 4c) and radiation (Figure 4e) induce higher evapotranspiration rates (see next section). Increases in low flows are expected for some subbasins and are likely due to increased subsurface liquid water content (see next section). The additional impact of land cover change is clear for the Athabasca and Peace basins, and consequently the Slave, and can be closely linked to glacier retreat

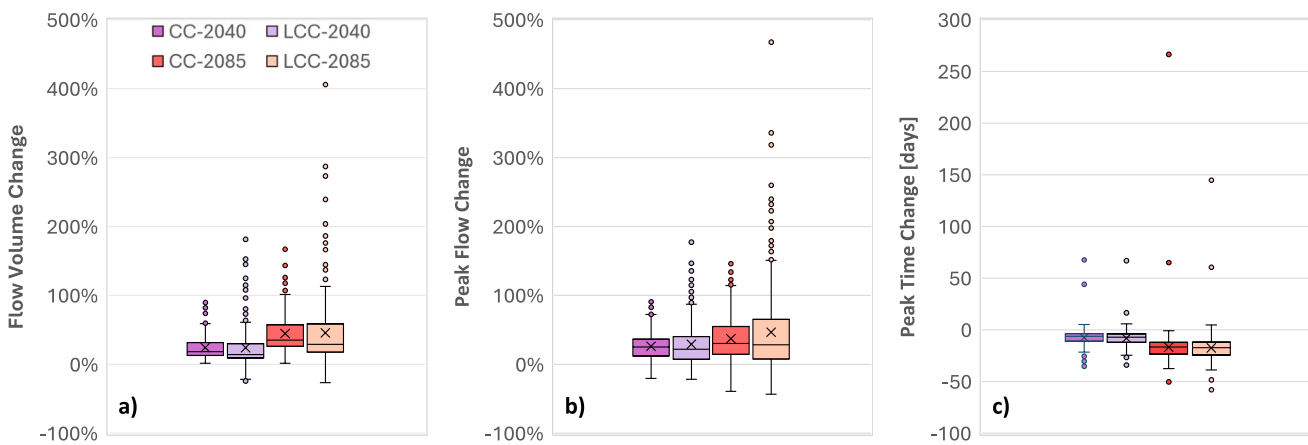


Figure 7. Box plots (a) relative changes to total volume, (b) relative changes in peak streamflow (daily climatological maximum), and (c) changes to peak time (time of the daily climatological maximum) for the Near and Far Future time slices for 277 stations (locations) within the MRB from the CanRCM4-WGC ensemble mean. Volume and peak flow changes are calculated as (Future/Baseline—1) while changes in timing are differences (Future—Baseline).

19447973, 2025, 12, Downloaded from https://agupubs.onlinelibrary.wiley.com/doi/10.1029/2024WR039276 by University Of Saskatchewan, Wiley Online Library on [08/12/2025]. See the Terms and Conditions (https://onlinelibrary.wiley.com/terms-and-conditions) on Wiley Online Library for rules of use; OA articles are governed by the applicable Creative Commons License

10.1029/2024WR039276

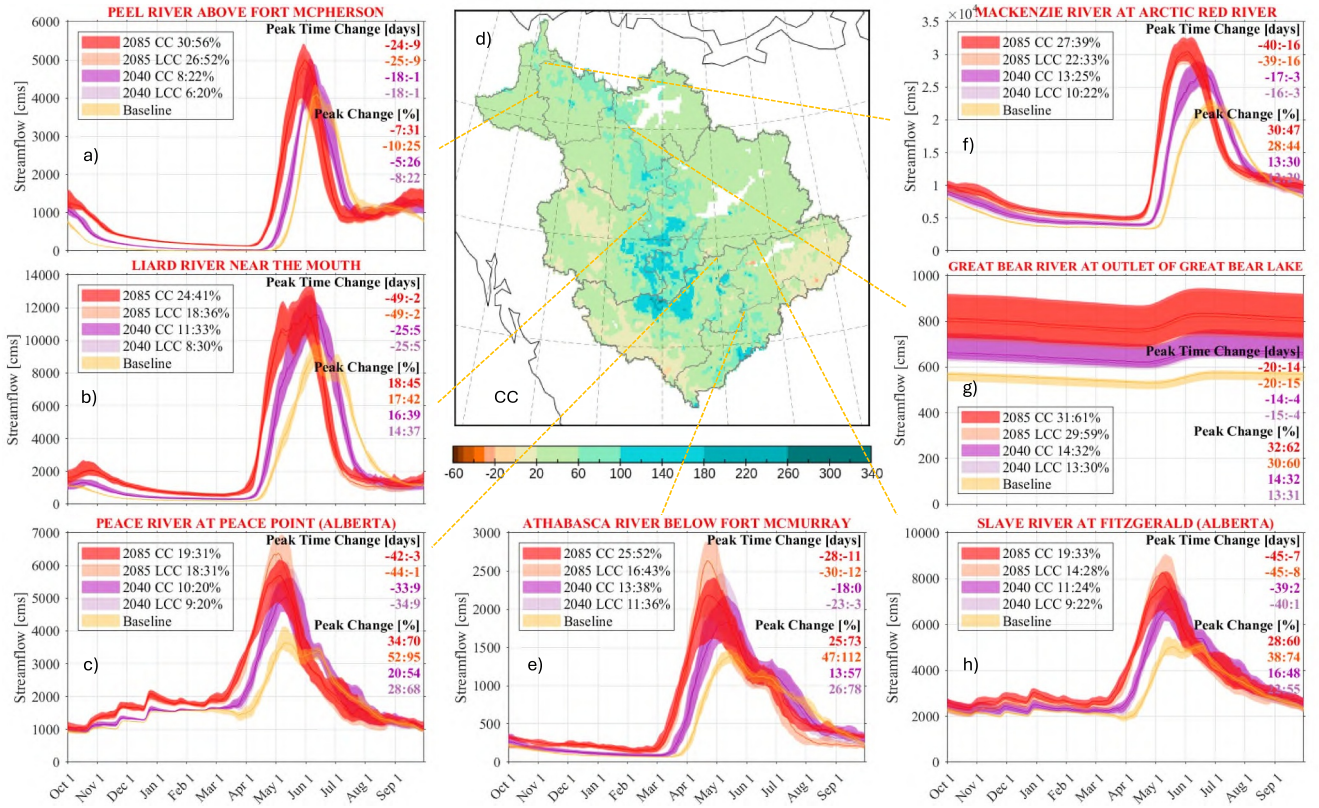


Figure 8. Simulated changes to hydrographs at key stations within the MRB under climate change (CC) and land cover change (LCC) for the Baseline, Near Future and Far Future time slices (30-year means). Gauge WSC names are shown in red above each panel with a dotted orange line connecting it to the map (d) to indicate location. Numbers in the legends of hydrographs indicate the flow volume changes (Future/Baseline—1) (%) as ranges across the ensemble (min:max). Changes to peak discharge values and timing are also indicated as ranges across the ensemble. The middle map (d) shows the spatial pattern of relative streamflow changes (%) for the ensemble mean for the far future time slice under CC.

as summer flows decline and spring peaks increase, compared to CC, due to diminishing icemelt and earlier snowmelt as glaciers diminish, as explained in Section 3.3. The additional impacts of LCC on streamflow elsewhere are small to negligible. The ensemble uncertainty bandwidth is highest around the peak (possibly heteroscedastic) and increases over time (i.e., 2085 has a wider bandwidth than 2040, whose is wider than the baseline's). The middle map (Figure 8d) shows the relative change (Future/Baseline −1) in streamflow as percentages for the far future under CC. A few spots show modest reductions while large areas around the Hay subbasin show significant relative increases.

CC generally increases the contribution of more northerly tributaries (e.g., Peel) than the southern ones (e.g., Athabasca) to the Mackenzie discharge to the Arctic Ocean as time progresses in the 21st century (Figure 9a). This is also indicated by the higher relative volume change shown in the legend of Figure 8 for Peel compared to the Athabasca, for instance. Compared to CC, the total discharge declines slightly under LCC (Figure 9b), due partly to reductions of glacier contributions, especially for the Athabasca and Peace in the far future but more generally due to increases in ET resulting from vegetation changes (see next sections), such as shrubs replacing tundra grasses and shifts in forest type as discussed in Section 3.2. Table S6 in Supporting Information S1 sheds more light on these changes and runoff coefficients under CC and LCC for the different subbasins. Overall, the shifts are not large, and the major contributors to the total streamflow of the Mackenzie River remain the Liard and the Peace tributaries.

4.2. Water Balance

Given the increase in precipitation (Figure 4a), both runoff (Figure 10a) and total subsurface moisture (Figure 11c) increase over time at the MRB scale. With the expected warming (Figure 4c), and the associated

19447973, 2025, 12, Downloaded from https://agupubs.onlinelibrary.wiley.com/doi/10.1029/2024WR039276 by University Of Saskatchewan, Wiley Online Library on [08/12/2025]. See the Terms and Conditions (https://onlinelibrary.wiley.com/terms-and-conditions) on Wiley Online Library for rules of use; OA articles are governed by the applicable Creative Commons License

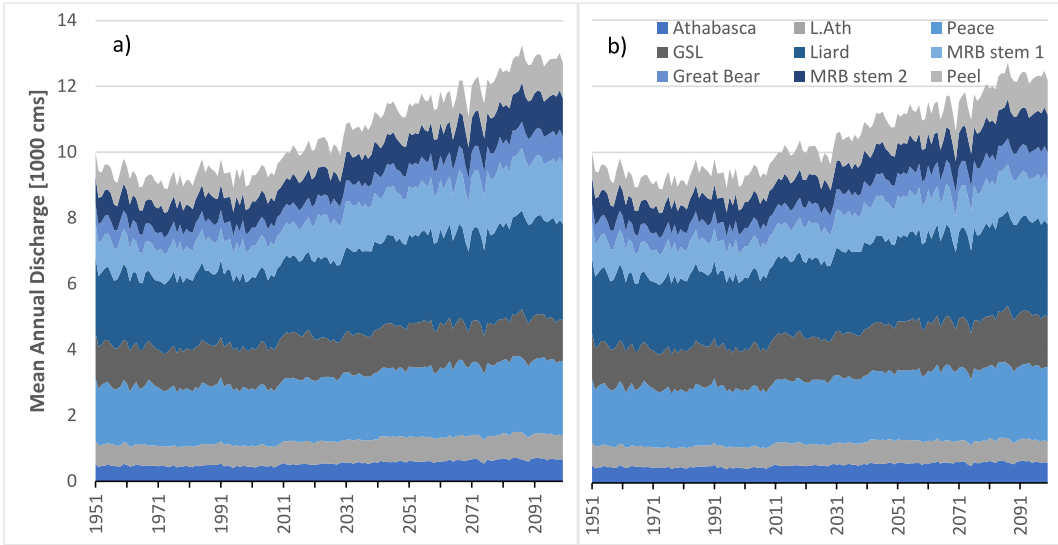


Figure 9. Mean annual time series of subbasin streamflow stacked to show contribution to total Mackenzie River streamflow from the ensemble mean of (a) CC Simulation, and (b) LCC simulations. See Figure 1 for subbasin delineation. The contribution of the Hay is included in the Great Slave Lake.

increase in incoming longwave radiation (Figure 4e), evapotranspiration (Figure 10c) also increases, especially during summer months (Figure 10d). The partitioning of precipitation into evapotranspiration and runoff (Figures 10e and 10f) shows only slight differences in their relative proportions favouring runoff over ET. The overall runoff coefficient of the MRB is simulated by the CanRCM4-WGC ensemble to be 36%–37% (which compares well with estimates based on CaPA precipitation and actual streamflow measurements near the basin outlet). The overall runoff coefficient only increases slightly to 36%–39% in the far future time slice under CC indicating that most of the runoff increase is a result of increasing precipitation, with increases in ET of similar proportion at the basin scale. The seasonal distribution of total runoff (Figure 10b) shows that the regime will remain dominated by snowmelt. LCC increases evapotranspiration slightly (Figures 10c and 10d) by about 2% for the far future compared to CC due to vegetation shifts as discussed above and in Section 3.2. This difference in ET is balanced by a slight reduction in runoff (5%–6% for the far future) (Figures 10a and 10b) under LCC compared to CC, leading to almost unchanged runoff coefficient under LCC. These basin-scale figures hide larger changes at the subbasin scale as shown in Sections S4 and S5 of Supporting Information S1 and in the spatial patterns of changes for ET and total runoff in Figures S9 and S10 of Supporting Information S1, respectively.

At the basin scale, there are some high mountains, mostly glaciated, that were covered by snow year-round during the baseline period (Figure 11b). This diminishes in the future as the length of the snow season shortens with warming. The annual average (Figure 11a) and peak SWE (Figure 11b) are slightly reduced although the timing of peak SWE does not show much change. However, the large MRB scale hides regional details that can be significantly different at the subbasin scale (see Section S5 in Supporting Information S1 for spatial patterns). Impacts of LCC on SWE at the basin scale are minimal.

The future increase in total subsurface moisture (Figures 11c and 11d) comes from a large increase in liquid water content (Figure 11h) at the expense of much reduced frozen content (Figure 11f), which occurs gradually over time (Figures 11e and 11g). In areas not underlain by permafrost (e.g., Athabasca and Peace subbasins), the length of the soil freezing season becomes shorter. Further North in areas underlain by permafrost (Section 4.4), degradation leads to deeper active layer prior to full permafrost thaw. Water previously locked as ice in those layers becomes liquid, which leads to generating higher runoff (mostly baseflow) and increases the availability of moisture for evapotranspiration by vegetation. Total subsurface moisture content is reduced slightly for LCC compared to CC suggesting greater plant water use with changing vegetation (Figures 11c and 11d).

MESH has three runoff components: surface overland flow, subsurface flow from all active subsurface layers which occurs due to having a sloped soil column, and baseflow from the bottom of the subsurface column (or at the soil-bedrock or soil-permafrost interface). All three components increase at the basin scale under CC, with the

19447973, 2025, 12, Downloaded from https://agupubs.onlinelibrary.wiley.com/doi/10.1029/2024WR039276 by University Of Saskatchewan, Wiley Online Library on [08/12/2025]. See the Terms and Conditions (https://onlinelibrary.wiley.com/terms-and-conditions) on Wiley Online Library for rules of use; OA articles are governed by the applicable Creative Commons License

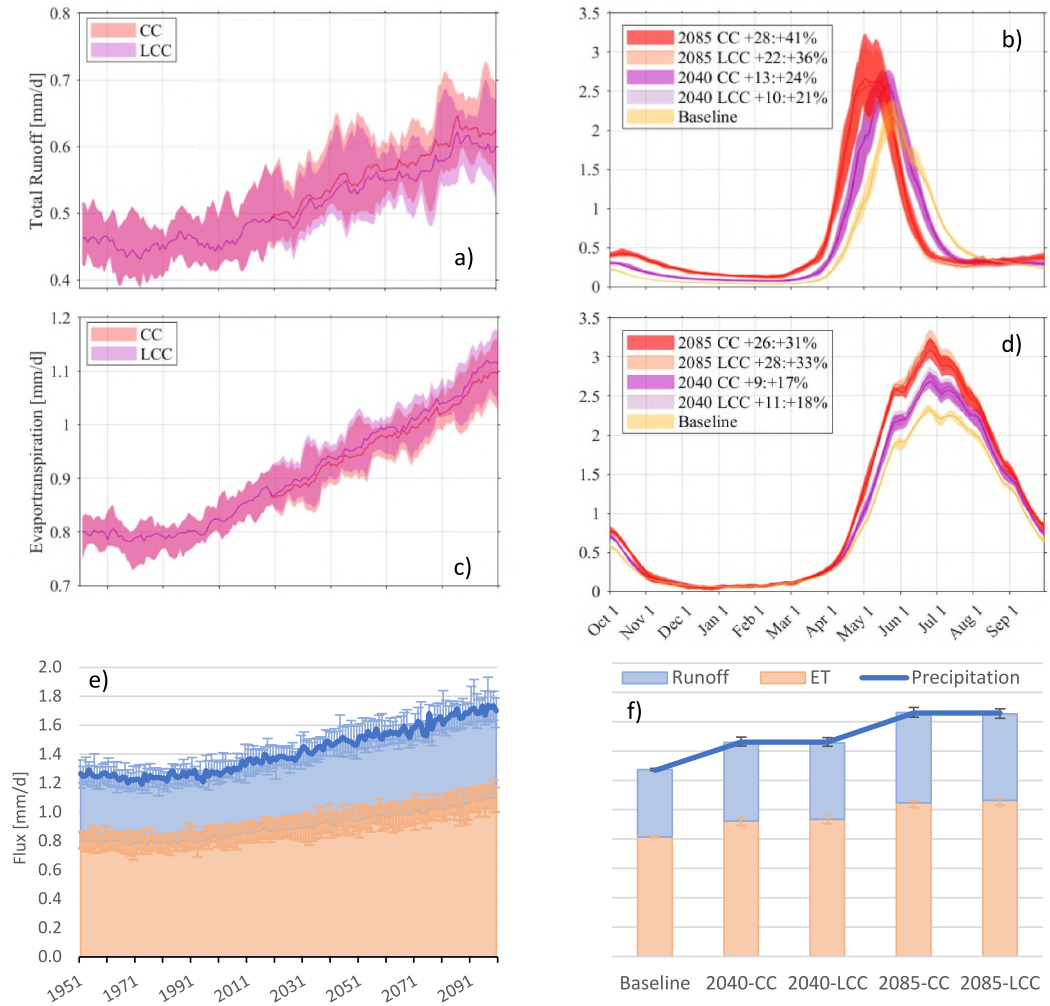


Figure 10. Simulated changes for the main water balance components (evapotranspiration and total runoff) averaged over the MRB under climate change (CC) and land cover change (LCC) scenarios. Panels (a, c) show the mean annual time series (smoothed by a 5-year filter) and panels (b, d) show seasonal distributions for the baseline (1981–2010), near future (2026–2055) and far future (2071–2100) (smoothed by a 10-day filter) with the range (min:max) of mean annual changes across the ensemble indicated in the legend. Panel (e) shows the time series of partitioning of precipitation into ET and runoff under CC while panel (f) shows how that partitioning changes in the near and far future for CC and LCC, with error bars shown for ET and Runoff to indicate the range across the ensemble.

largest relative increases at the annual time scale occurring for the baseflow (groundwater) component (Figures 12a, 12b and 12e). This aligns with the increase of liquid subsurface moisture content and increased lateral connectivity. Compared to CC, total runoff increases are slightly less under LCC due to the loss of glaciers reducing overland flow (Figures 12b and 12c) in late summer, and due to reductions in interflow and baseflow all year round (Figures 12b and 12e) due to increased evapotranspiration. The different partitioning of runoff in the future may have implications for the quality of river streamflow depending on the available minerals and biological activity within those deeper subsurface layers and degrading permafrost. Figures S11–S13 in Supporting Information S1 show the spatial patterns of change for runoff components.

4.3. Glaciers

The overall glacier contribution at the MRB outlet is very small, amounting to only 0.47% of the total runoff volume for the ensemble mean at the outlet for the baseline period; this is reduced to 0.41% and 0.07% for the near and far future time slices when glacier retreat is considered. Even when glacier retreat is ignored and CC is applied

19447973, 2025, 12, Downloaded from https://agupubs.onlinelibrary.wiley.com/doi/10.1029/2024WR039276 by University Of Saskatchewan, Wiley Online Library on [08/12/2025]. See the Terms and Conditions (https://onlinelibrary.wiley.com/terms-and-conditions) on Wiley Online Library for rules of use; OA articles are governed by the applicable Creative Commons License

10.1029/2024WR039276

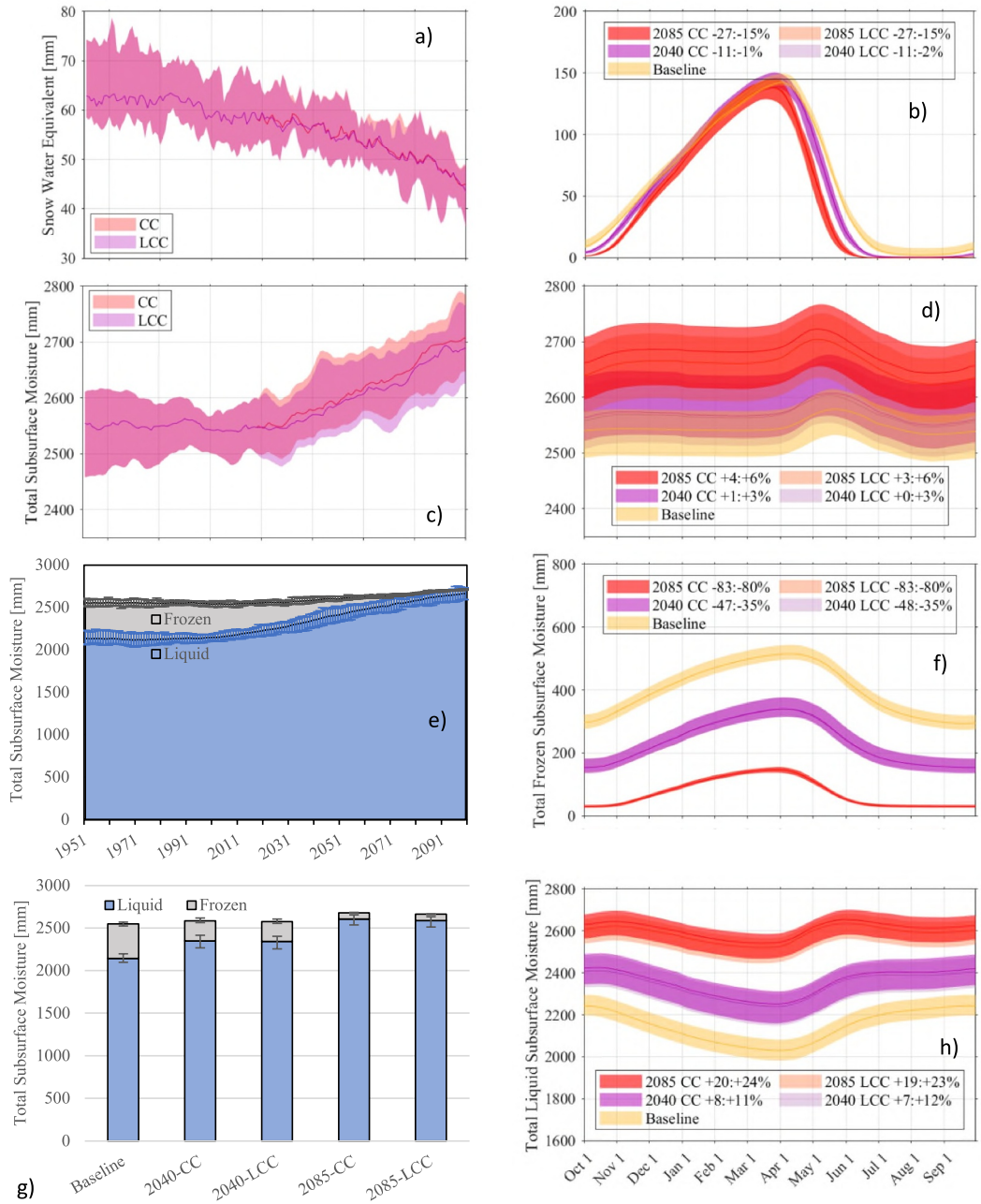


Figure 11. Simulated changes for main storage components of snow and subsurface moisture using the CanRCM4-WGC ensemble averaged over the MRB under climate change (CC) and land cover change (LCC) scenarios. Panels (a, b) show the time series (smoothed by a 5-year filter) and seasonal distributions for the baseline (1981–2010), near future (2026–2055) and far future (2071–2100) (smoothed by a 10-day filter) for snow. Panels (c, d) show the same for total subsurface water content. Panel (e) shows the time series for the liquid and frozen subsurface water content stacked for CC ensemble mean while panels (f, h) show the seasonal distributions for liquid and frozen contents, respectively similar to (b, d). Panel (g) shows stacked climatological ensemble means of these components for the baseline, near future and far future periods under CC and LCC. Bands on panels (a–d, f and h) indicate the uncertainty range across the ensemble and values in the legend of right panels indicate the relative change (1—Future/Baseline) (%) as ranges across the ensemble (min:max). Error bars on panels (e, g) indicate the uncertainty range across the ensemble. Liquid and frozen water contents are integrated for all sub-surficial layers.

19447973, 2025, 12, Downloaded from https://agupubs.onlinelibrary.wiley.com/doi/10.1029/2024WR039276 by University Of Saskatchewan, Wiley Online Library on [08/12/2025]. See the Terms and Conditions (https://onlinelibrary.wiley.com/terms-and-conditions) on Wiley Online Library for rules of use; OA articles are governed by the applicable Creative Commons License

10.1029/2024WR039276

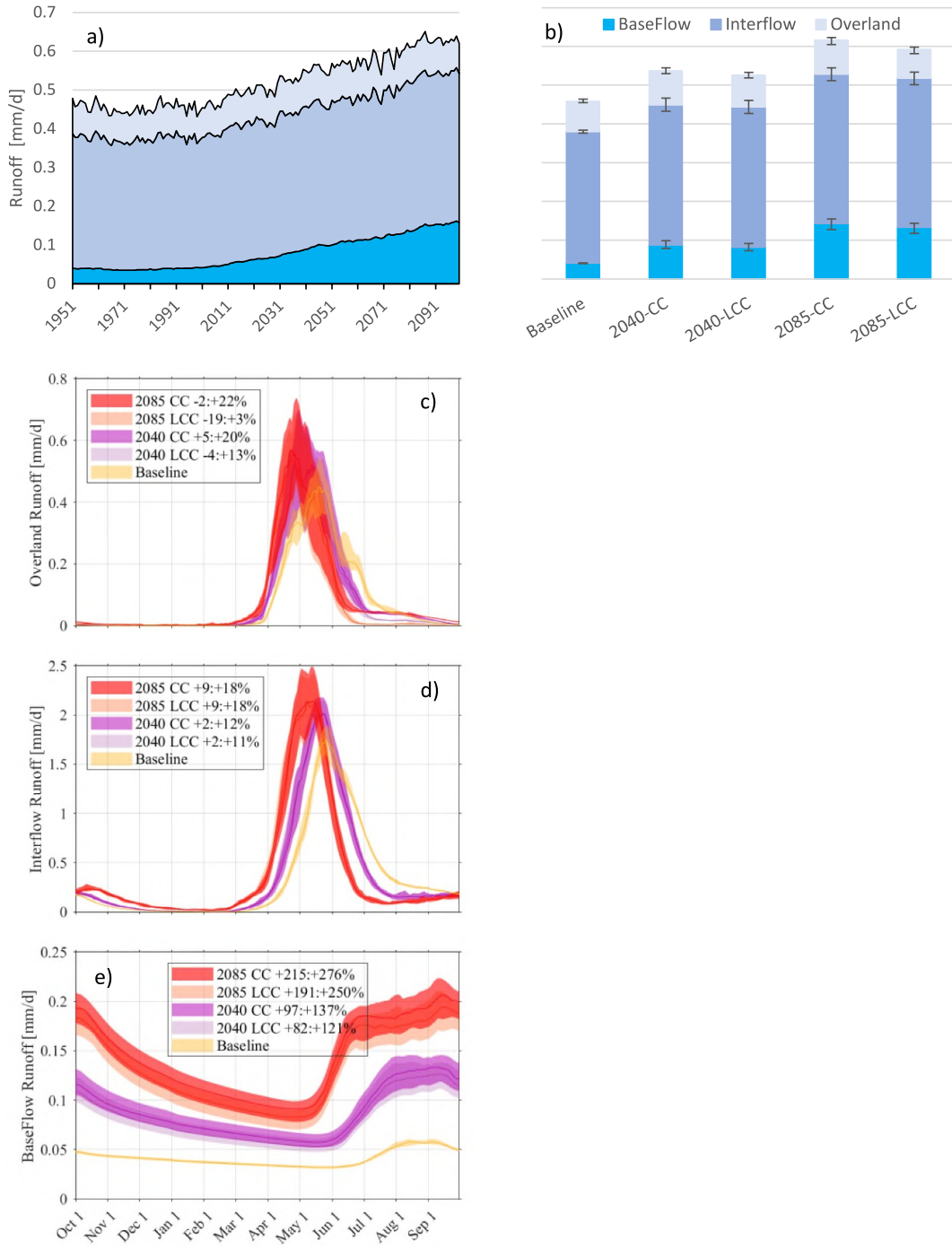


Figure 12. Simulated changes for the runoff components using the CanRCM4-WGC ensemble averaged over the MRB. Panel (a) shows the annual time series of the three components for the ensemble mean under CC. Panel (b) shows stacked climatological ensemble means of the three components for the baseline (1981–2010), near future (2026–2055) and far future (2071–2100) under CC and LCC; ensemble spread is shown as error bars. Panels (c, d, e) show the seasonal distributions (smoothed by a 10-day filter) for overland runoff, interflow (subsurface runoff integrated over all layers), and baseflow (largely groundwater flow) respectively under CC and LCC. Bands indicate the uncertainty range and values in the legend indicate the relative change (1—Future/Baseline) across the ensemble (min:max).

19447973, 2025, 12, Downloaded from https://agupubs.onlinelibrary.wiley.com/doi/10.1029/2024WR039276 by University Of Saskatchewan, Wiley Online Library on [08/12/2025]. See the Terms and Conditions (https://onlinelibrary.wiley.com/terms-and-conditions) on Wiley Online Library for rules of use; OA articles are governed by the applicable Creative Commons License

holding glaciated areas fixed, the contribution increases to only 1% and 1.46% for the ensemble mean. Although unrealistic, this represents an upper limit for any "peak water" glacier contribution at the entire basin scale under the studied climate change scenario.

However, glaciers are important at the scale of the headwater catchments where they cover a larger fraction of the subbasin and further downstream as they provide a considerable contribution to the total annual runoff compared to their area. Additionally, that contribution comes in late summer when evapotranspiration downstream is highest whilst the snow melt peak has passed, and river flows are generally receding, except for contributions from rainfall-runoff events. They also have a temperature regulating effect in late summer that may have ecological consequences in some regions. To exemplify the important contribution of glaciers, a small headwater basin (Athabasca above Jasper—Station 07AA002, see Figure S6 in Supporting Information S1 for location) is considered. This Canadian Rockies subbasin has an area of 3,870 km^2, 6% of which is glaciated, contributing 13.2% to the total annual runoff volume during the baseline period (ensemble mean). Considering both glacier retreat and climate change (LCC), this contribution increases in the near future to 21.8% of the total annual runoff, demonstrating some peak water attributes, before reducing in the far future to only 10.7% for the ensemble mean. The glacier contribution diminishes at the outlet of the Athabasca (station 07DA001) in northern Alberta to only 2.5%, 3.4%, and 1.1% for the baseline, near future, and far future time slices for the ensemble mean under LCC. Section S4 in Supporting Information S1 sheds more light on glacier contribution along other main tributaries and along the Mackenzie main stem and how it is expected to change in the future.

4.4. Permafrost

The extent of permafrost is expected to decline significantly over time (Figure 13), with most of the reduction occurring later in the century. The trend of permafrost loss accelerates during the period 2030–2085 after a slower decline during 2000–2030 (Figure 14). This occurs over all ensemble members and the range of uncertainty becomes smaller with time, that is, ensemble members converge, despite the large initial spread in 1951 that originates from model initialization via cycling the first 10 years of climate forcing independently for each ensemble member. By the end of the century, it is expected that only areas around the far northern Peel River and Mackenzie Delta (which are currently in the continuous permafrost zone) will remain underlain by patches of permafrost, around 3%–5% of the MRB area in 2100, compared to about 36%–44% in 1951. A tile (a specific GRU in a specific model grid cell) is deemed to have permafrost if at least one subsurface layer (out of the modelled 25 layers down to 51.24 m depth) remains cryotic all year round (slightly deviates from the standard 2-year definition to simplify calculations). The southern limit of permafrost is pushed northwards and only a few patches around and south of 60°N are expected to remain underlain by permafrost due to a high soil organic content, which is assumed to remain unchanged. Wildfire is not integrated into the model and severe and more frequent fires are expected in the future which can burn organic layers (Johnstone et al., 2010). The rates of permafrost loss are lower than those of Aalto et al. (2018), predicted by statistical models, but these have no consideration of organic soils. The permafrost area loss curve (Figure 14) agrees with previous global results based on CMIP5 (e.g., Koven et al., 2013) and CMIP6 (e.g., Burke et al., 2020). There is a negligible impact from LCC compared to CC and thus LCC results are not shown. Glaciers are assumed to be underlain by permafrost in MESH, and with their retreat, mountains show as permafrost free in the future (see the far future panels of Figure 13). Note that the ensemble statistics shown in Figure 13 were calculated at the grid cell level and thus do not represent any specific ensemble member; they are likely to be more extreme than any specific member.

As shown above, permafrost thaw is significant across the basin and accelerates over time, leaving most of the basin permafrost-free by the end of the 21st century. Meanwhile, runoff increases in the future with baseflow contributions showing the highest relative change compared to the baseline. To explore the linkages between permafrost thaw and runoff changes, runoff components of three subbasins of the MRB were investigated. The basins are the Athabasca, which is almost permafrost free during the baseline, the Liard, which lies in the sporadic and discontinuous permafrost zones, and the Peel, which is underlain by continuous permafrost for the baseline and near future and will remain partially underlain by permafrost in the far future (see Figure 13). For the Athabasca, overland flow (Figure 15g) increases slightly mid-century then declines with a greater reduction under LCC due to deglaciation. A similar trend can be seen for the Liard (Figure 15d), whilst the Peel (Figure 15a) shows mostly a downward trend with almost no difference between CC and LCC. Interflow increases over time for the Athabasca (Figure 15h) but shows no persistent trend for the Liard or the Peel (Figures 15e and 15b). LCC does not make much difference to any of the three basins. More persistent rising trends are expected for the

19447973, 2025, 12, Downloaded from https://agupubs.onlinelibrary.wiley.com/doi/10.1029/2024WR039276 by University Of Saskatchewan, Wiley Online Library on [08/12/2025]. See the Terms and Conditions (https://onlinelibrary.wiley.com/terms-and-conditions) on Wiley Online Library for rules of use; OA articles are governed by the applicable Creative Commons License

10.1029/2024WR039276

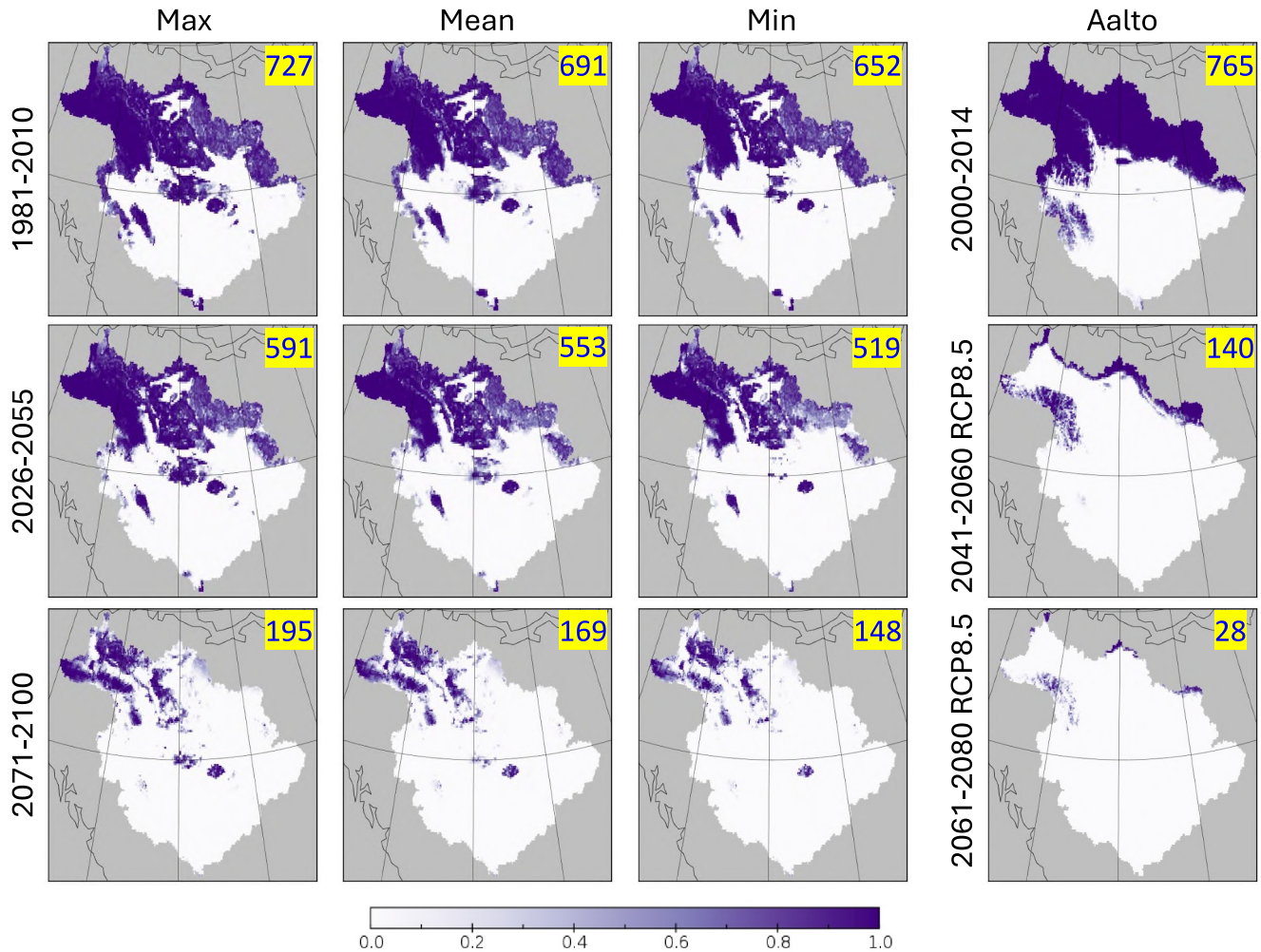


Figure 13. Simulated Changes in 30-year mean permafrost probability for the baseline (1981–2010), Near Future (2026–2055) and Far Future (2071–2100) showing the CanRCM4-WGC ensemble max, mean, and min (calculated at the grid cell level) compared to results from Aalto et al. (2018) for RCP8.5. Permafrost area in (1,000 km^2) is shown in the yellow box in the top right corner of each panel, calculated as the sum of GRU fractions underlain by permafrost times the grid cell area.

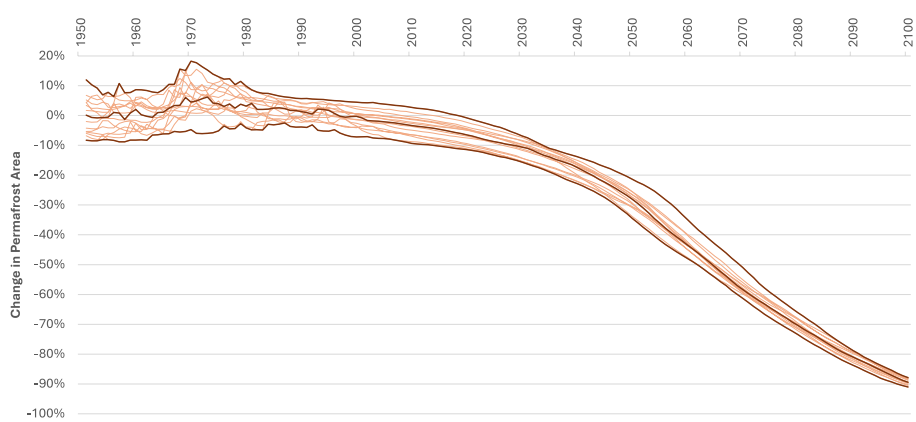


Figure 14. Change to Permafrost Area across the MRB over the full simulation period (1951–2100) compared to the ensemble mean over the baseline (1981–2010). Each light line represents one ensemble member of CanRCM4-WGC; dark lines indicate the ensemble max, min, and median.

19447973, 2025, 12, Downloaded from https://agupubs.onlinelibrary.wiley.com/doi/10.1029/2024WR039276 by University Of Saskatchewan, Wiley Online Library on [08/12/2025]. See the Terms and Conditions (https://onlinelibrary.wiley.com/terms-and-conditions) on Wiley Online Library for rules of use; OA articles are governed by the applicable Creative Commons License

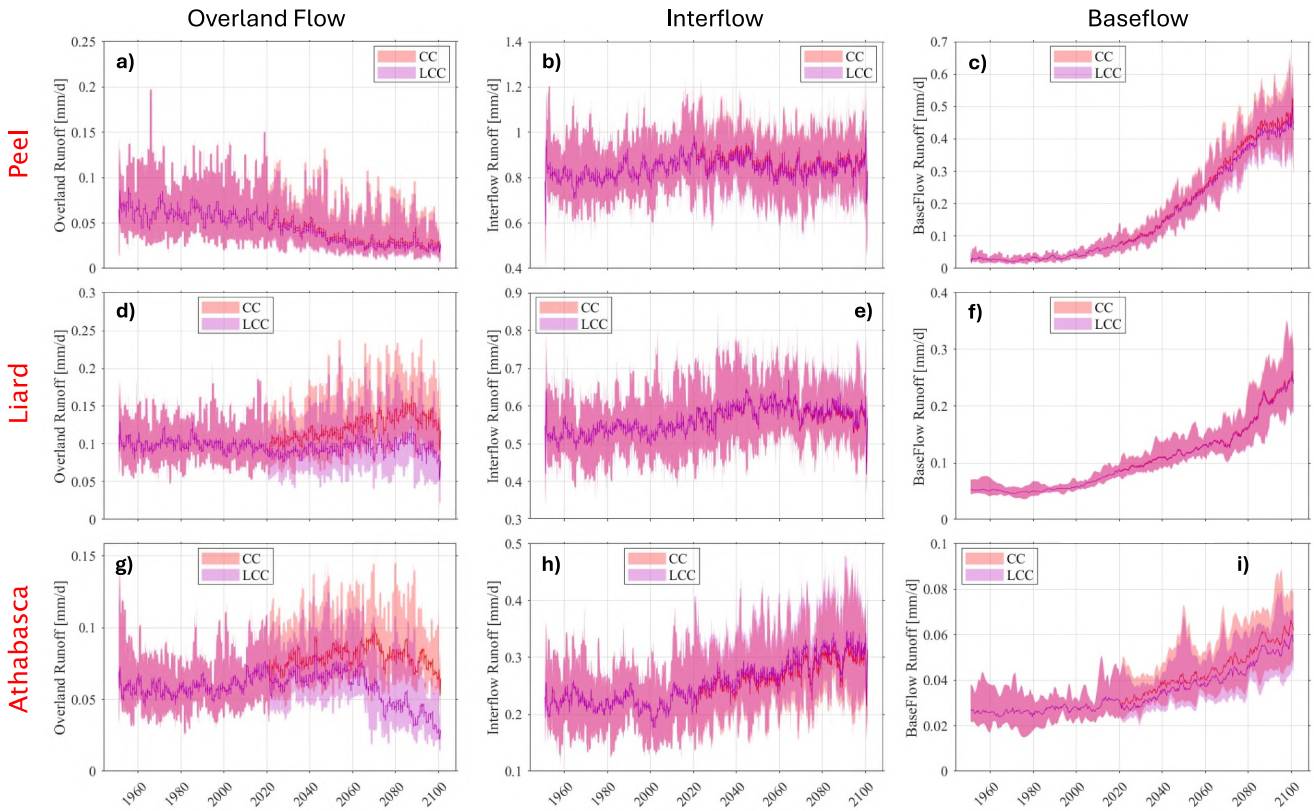


Figure 15. Annual timeseries of subbasin averaged runoff components under CC and LCC scenarios for three selected subbasins. Bands show the spread (min:max) across the CanRCM4-WGC ensemble.

baseflow for all three subbasins (Figures 15c, 15f and 15i). The important feature is that greater increases are expected for the Peel than for the Liard, which, in turn, has greater increases than the Athabasca. As mentioned in Section 4.2, frozen subsurface water content is greatly reduced basin-wide at the expense of increasing liquid content and thus subsurface water is mobilized to contribute more to runoff, mostly as baseflow through newly unfrozen subsurface flow pathways. Moving north from the Athabasca to the Liard, and then to the Peel, permafrost thaw contributes additional subsurface moisture mobility and connectivity and thus, increases in baseflow become larger. Interflow did not increase due to permafrost thaw, possibly due to the horizontal hydraulic conductivity diminishing sharply with depth as is well known in the region (Carey et al., 2007). Thus, with permafrost thaw, excess subsurface liquid water percolates downwards to contribute to baseflow rather than flowing laterally to contribute to interflow. In most cases, the depth to bedrock is deep enough not to limit interflow. Figures S11–S13 in Supporting Information S1 show the spatial patterns of change for runoff components.

5. Conclusions and Recommendations

5.1. Summary of Projected Changes

Climate change scenarios from the CanRCM4-WGC ensemble (15 members) were used to drive a high-fidelity MESH model of the MRB over the period 1951–2100. The model was run using a deep subsurface profile (51 m) and proper initialization procedure to simulate permafrost dynamics in addition to hydrological fluxes. The CanRCM4-WGC ensemble was constructed through bias correcting 15 members of previously dynamically downscaled CanESM2 simulations that were forced by the RCP 8.5 emission scenario. To account for concurrent changes in land cover, a land cover change scenario, including glacier retreat, was constructed using the potential change signal (Rehfeldt et al., 2012) in response to climate change, and expert knowledge- constrained vegetation migration including triggers such as wildfire. The land cover change (LCC) scenario was implemented as changes

19447973, 2025, 12, Downloaded from https://agupubs.onlinelibrary.wiley.com/doi/10.1029/2024WR039276 by University Of Saskatchewan, Wiley Online Library on [08/12/2025]. See the Terms and Conditions (https://onlinelibrary.wiley.com/terms-and-conditions) on Wiley Online Library for rules of use; OA articles are governed by the applicable Creative Commons License

19447973, 2025, 12, Downloaded from https://agupubs.onlinelibrary.wiley.com/doi/10.1029/2024WR039276 by University Of Saskatchewan, Wiley Online Library on [08/12/2025]. See the Terms and Conditions (https://onlinelibrary.wiley.com/terms-and-conditions) on Wiley Online Library for rules of use; OA articles are governed by the applicable Creative Commons License

to GRU fractions at two specified times (2021 and 2066) to simplify the simulation workflow. Analysis for CC and LCC focused on two 30-year future time slices: 2026–2055 as near future, and 2071–2100 as far future, in comparison to a 30-year historical time slice: 1981–2010 as the baseline.

In general, higher rainfall is expected over most of the MRB because of warming. Although the increase in temperature, and the associated changes in radiation and humidity are expected to raise evapotranspiration (ET), the balance indicates expected increases in streamflow volumes and peaks. Streamflow is expected to peak earlier by 2–3 weeks on average by the end of the 21st century for most subbasins in response to earlier snowmelt and higher spring precipitation, mostly expected to fall as rain. As a result of hydrograph shifts, some reaches could experience reduced summer flows which can pose challenges for water management and navigation, for example, Glacier retreat will further accentuate the above changes for the Athabasca and Peace subbasins, especially for their headwaters where the glacier contribution to discharge is currently significant. This calls for a different management strategy of existing reservoirs and possibly the construction of additional ones to manage the low summer flows. Further downstream along those rivers, along other rivers and along the main Mackenzie, the additional impact of LCC is a relatively small reduction in discharge but with greater uncertainty. The glacier contribution to the Mackenzie discharge at the outlet is already very small and will become negligible with further deglaciation and climate change.

The expected changes to streamflow hydrographs are closely linked to changes in water balance components. As mentioned above, ET is expected to increase by 26%–31% for the far future at the MRB scale but also subsurface moisture is expected to increase. The most significant change to subsurface moisture is the shift towards having much more liquid content at the expense of much reduced frozen content. Liquid content is mobile and contributes to the increase in ET, but also to the increase of baseflow runoff contribution to total runoff, despite increases to the other two components (overland flow and interflow). The snow season is expected to be shorter, that is: larger regions are expected to experience snow-free conditions for longer. Peak snow at the basin scale is expected to be slightly lower and to occur earlier in the spring.

Under warming, permafrost is expected to thaw rapidly across all zones, even the continuous one. The rate of permafrost loss accelerates from 2030 to 2090 after a slower rate earlier. By the end of the century, only 10% of the area currently underlain by permafrost is expected to survive due to either its location (far north and north-west) or its organic-rich soil, assuming these soils will not undergo mineralization following severe fires. The implications of such widespread permafrost thaw are expected to be significant for northerly communities who rely on cryotic ground for their infrastructure and livelihoods and for terrestrial ecosystems where upland forests may experience thermokarst collapse due to thaw of ice rich permafrost. A shift from the traditional "keep it frozen" to "let it thaw" in infrastructure design maybe necessary to accommodate the changing permafrost conditions.

As discussed above, the baseflow component of runoff registers the largest relative increase of all runoff components at the MRB scale. This remains true at the subbasin scale but in connection with permafrost thaw, the increase in baseflow is expected to be larger moving northwards, especially in the far future. The additional subsurface water mobility in thawed areas allows for larger quantities of liquid water to percolate contributing to baseflow. While the increased connectivity could have also resulted in increasing interflow, the model horizontal conductivity declined rapidly with depth, and thus it becomes more likely for the increased liquid content to seep downwards (contributing to baseflow) than to flow laterally as interflow.

5.2. Uncertainty and Variability

The 15-member CanRCM4-WGC ensemble is based on a single emissions scenario (RCP8.5) and comes from a single chain of models. Therefore, only one source of uncertainty is accounted for in the simulations. The uncertainty bandwidth shown for all results originates from the initial condition perturbations performed when the CanESM2 and CanRCM4 simulations were conducted (Section 3.1) and does not include uncertainties due to emission scenarios or modelling uncertainties across the range of models used, starting from the global to the regional climate models, down to the impact model (MESH). The computational expenses to conduct a multi-scenario and multi-model ensemble are huge for a basin of this size at the current discretization scale.

However, warming following RCP8.5 is plausible as methane emissions have been underestimated (Yu et al., 2023) and most countries are well below, or have abandoned, their pledges for the Paris agreement

19447973, 2025, 12, Downloaded from https://agupubs.onlinelibrary.wiley.com/doi/10.1029/2024WR039276 by University Of Saskatchewan, Wiley Online Library on [08/12/2025]. See the Terms and Conditions (https://onlinelibrary.wiley.com/terms-and-conditions) on Wiley Online Library for rules of use; OA articles are governed by the applicable Creative Commons License

(Roelfsema, 2020) whilst socio-economic development and cumulative emissions remain consistent with this scenario (Schwalm et al., 2020). The climate forcings were bias corrected to ensure they correspond to current climate, and the fidelity of the impact model has been assessed thoroughly not only for streamflow but also for permafrost and other fluxes and states. Therefore, the results shown are thought to be plausible and credible enough to project the future of the MRB. Additionally, they are detailed enough to allow for adaptation planning at the subbasin scale. Section S5 in Supporting Information S1 sheds more light on the spatial patterns of future changes.

Nevertheless, it is known that CanESM2 equilibrium climate sensitivity of 3.7 K is higher than CMIP5 models' mean (Schlund et al., 2020) and therefore it is likely projecting higher changes than the CMIP5 ensemble mean but it is by no means an outlier. Evaluation of the CMIP5 ensemble (Sheffield, Barrett, et al., 2013; Sheffield, Camargo, et al., 2013) against observations show that CanESM2 is a credible model despite biases in some climatic features (e.g., summer temperature overestimation) which are mostly removed prior to using its downscaled output (using CanRCM4) for forcing the MRB model. Additionally, the results of this study were compared to those of another similar study conducted using 3 MESH parametrizations for the Liard subbasin. Abdelhamed (2023) used a larger forcing ensemble comprised of statistically downscaled and bias corrected output from 10 CMIP6 ESMs forced with 3 Socio Economic Pathways (SSPs: SSP585, SSP370 and SSP126) from the Inter-Sectoral Impact Model Intercomparison Project 3b (ISIMIP3b: Lange, 2019) yielding a 90-member ensemble run for the future period 2015–2100. Comparisons of streamflow and permafrost area timeseries from the CanRCM4-WGC versus ISIMIP3b are shown in Section S6 of Supporting Information S1. As expected, the CanRCM4-WGC ensemble spread is narrower than that of Abdelhamed's ensemble for both streamflow (at the Liard outlet) and permafrost area over the subbasin. Changes to streamflow are mostly comparable but reductions for permafrost area from the CanRCM4-WGC ensemble are more severe than the larger ensemble even when considering SSP585 (which uses RCP8.5 for emissions) only. Additionally, the spread of the larger ensemble increases in the future while CanRCM4-WGC converges to near permafrost-free conditions for the Liard subbasin. There are differences regarding model parameterization and initialization between the two ensembles that are discussed in Section S6 of Supporting Information S1.

Additionally, a single land cover change scenario was used. Constructed to be compatible with the CC ensemble it is constrained to be plausible with RCP8.5, and it does not capture the width of possible changes. It was also integrated with a single glacier retreat scenario based on results for the same modelling chain (ESM2-RCP8.5) provided by Clarke et al. (2015). The land cover change scenario was also introduced abruptly at two specific times. To be able to consider other RCPs or SSPs, and explore the full range of uncertainty in a fully transient simulation, the framework needs to include vegetation dynamics that integrate or couple ecological drivers such as pests, disease, and wildfires, which alters the natural species competition used in dynamic vegetation models (e.g., CLASS-CTEM: Arora et al., 2018). Additionally, glacier dynamics, including firnification (Pradhananga & Pomeroy, 2022) and changes to ice extents and albedo (Aubry-Wake et al., 2022) need to be considered to better predict transient changes in the mountain headwaters.

Spatial, inter-annual and seasonal climate variability is also encompassed by the modelling framework used. While changes to seasonal streamflow and water balance patterns are shown and discussed in results, inter-annual variability is shown implicitly in the time series plots (e.g., Figures 4, 9 and 15). Section S5 in Supporting Information S1 sheds more light on how spatial variability is expected to change in the future.

5.3. Limitations and Future Directions

This study followed a modelling chain approach that starts with ESM simulations downscaled by an RCM and bias corrected to force a physically based hydro-cryosphere LSM with strong emphasis on cold regions processes. As such, it provided high fidelity spatially distributed change patterns for several hydrological and cryosphere states and fluxes over the vast MRB under climate change, land cover change, and management scenarios to guide adaptation. However, in addition to the limitations discussed above regarding the cascade of uncertainty, the modelling chain, and particularly the utilized H-LSM (MESH) can be improved in several ways.

Some of the model physics can be further improved. For example, full consideration of slope, aspect and elevation bands can improve the simulations in mountain headwaters (Tesemma et al., in review) in addition to incorporating fully dynamic glaciers including firnification (Pradhananga & Pomeroy, 2022). Improvements to the water and energy balance of water bodies via incorporation of small lakes (Garnaud et al., 2022) and coupling to

19447973, 2025, 12, Downloaded from https://agupubs.onlinelibrary.wiley.com/doi/10.1029/2024WR039276 by University Of Saskatchewan, Wiley Online Library on [08/12/2025]. See the Terms and Conditions (https://onlinelibrary.wiley.com/terms-and-conditions) on Wiley Online Library for rules of use; OA articles are governed by the applicable Creative Commons License

hydrodynamic lake models for the three large lakes within the basin (similar to the Dupont et al. (2012) application of NEMO to the Great Laurentian lakes) are also important. Recent developments in CLASSIC (Melton et al., 2020), a successor to CLASS, have introduced a specific sub-model for shrubs (Meyer et al., 2021), which would also improve the simulations when incorporated in MESH. Coupling to river ice models to include the effects of ice jams (Zhang et al., 2022) can allow better predictions of river stage and flooding events. Improvements to frozen soil algorithms (Krogh & Pomeroy, 2021) and incorporation of freezing point depression (Amankwah et al., 2021) and other enhancements to the subsurface thermodynamics can further improve permafrost predictions and their associated impacts on hydrology.

In addition to improving the model physics, improvements to computational efficiency, spatial resolution, and parameters are needed. In this regard, conditioning parameters using remotely sensed data sets such as the Gravity Recovery and Climate Experiment (GRACE: Tapley et al., 2004) terrestrial water storage following Yassin et al. (2017) and/or the Surface Water and Ocean Topography (SWOT: Chen, 2023) lake and river water levels may be helpful. This may require a shift from the GRU approach in specifying parameters to other hybrid methods that utilize spatial data sets when accurate ones are available, as done for the model used in this study for soil texture and a few other parameters (Elshamy et al., 2025). With the move towards higher resolution and vector-based routing in HLSMs (e.g., Vanderkelen et al., 2022), further investigations are necessary for the effects of discretization scale on parametrizations which requires fine-scale observations of water and energy fluxes and states for model development and evaluation. Finally, CMIP6 bias-corrected and downscaled realizations are now mostly available for the region (Paquin et al., 2024) and must be considered for any future runs.

Conflict of Interest

The authors declare no conflicts of interest relevant to this study.

Data Availability Statement

Model setup, run scripts and MESH code used to produce the results of this study are available at https://zenodo.org/records/15741525. Data sets used to build the model are referenced in Section 2.3 with additional references given in Elshamy et al. (2025). The meteorological forcing data (CanRCM4-WGC) was made available at https://doi.org/10.20383/103.0622 (Asong et al., 2022).

Acknowledgments
This research started as part of the Changing Cold Region Network, funded by Canada's Natural Science and Engineering Research Council and by the Canada Excellence Research Chair in Water Security at the University of Saskatchewan. The research continued under the Global Water Futures programme funded by Canada First Research Excellence Fund. Gratitude is expressed to the many scientists in the Government of Canada and many Canadian universities who participated in the development of the MESH modelling framework and to the many scientists, technicians and agencies who developed the scientific understanding and collected field data used to evaluate and improve this model. The input of two anonymous reviewers to the manuscript is gratefully acknowledged.

References

Aagaard, K., & Carmack, E. C. (1989). The role of sea ice and other fresh water in the Arctic circulation. *Journal of Geophysical Research*, *94*(C10), 14485–14498. https://doi.org/10.1029/JC094iC10p14485

Aalto, J., Karjalainen, O., Hjort, J., & Luoto, M. (2018). Statistical forecasting of current and future Circum-Arctic ground temperatures and active layer thickness. *Geophysical Research Letters*, *45*(10), 4889–4898. https://doi.org/10.1029/2018GL078007

Abdelhamed, M. S. (2023). Towards improved hydrologic land-surface modelling to represent permafrost. https://hdl.handle.net/10388/14972

Abdelhamed, M. S., Razavi, S., Elshamy, M. E., & Wheater, H. S. (2024). Assessment of a hydrologic-land surface model to simulate thermo-hydrologic evolution of permafrost regions. *Journal of Hydrology*, *645*, 132161. https://doi.org/10.1016/j.jhydrol.2024.132161

Abdelmoaty, H. M., Papalexiou, S. M., Rajulapati, C. R., & AghaKouchak, A. (2021). Biases beyond the mean in CMIP6 extreme precipitation: A global investigation. *Earth's Future*, *9*(10), e2021EF002196. https://doi.org/10.1029/2021EF002196

Agyeman, R. Y. K., Huo, F., Li, Z., & Li, Y. (2021). Modelled changes in selected agroclimatic indices over the croplands of western Canada under the RCP8.5 scenario. *Quarterly Journal of the Royal Meteorological Society*, *147*(741), 4454–4467. https://doi.org/10.1002/QJ.4188

Agyeman, R. Y. K., Huo, F., Li, Z., Li, Y., Elshamy, M. E., & Hwang, Y. (2023). Impact of climate change under the RCP8.5 emission scenario on multivariable agroclimatic indices in Western Canada from convection-permitting climate simulation. *Anthropocene*, *44*, 100408. https://doi.org/10.1016/j.ancene.2023.100408

Alexeev, V. A., Nicolsky, D. J., Romanovsky, V. E., & Lawrence, D. M. (2007). An evaluation of deep soil configurations in the CLM3 for improved representation of permafrost. *Geophysical Research Letters*, *34*(9), L09502. https://doi.org/10.1029/2007GL029536

Amankwah, S. K., Ireson, A. M., Maulé, C., Brannen, R., & Mathias, S. A. (2021). A model for the soil freezing characteristic curve that represents the dominant role of salt exclusion. *Water Resources Research*, *57*(8), e2021WR030070. https://doi.org/10.1029/2021WR030070

Arora, V. K., Melton, J. R., & Plummer, D. (2018). An assessment of natural methane fluxes simulated by the CLASS-CTEM model. *Biogeosciences*, *15*(15), 4683–4709. https://doi.org/10.5194/bg-15-4683-2018

Arora, V. K., Scinocca, J. F., Boer, G. J., Christian, J. R., Denman, K. L., Flato, G. M., et al. (2011). Carbon emission limits required to satisfy future representative concentration pathways of greenhouse gases. *Geophysical Research Letters*, *38*(5). https://doi.org/10.1029/2010GL046270

Asong, Z. E., Elshamy, M. E., Princz, D., Wheater, H. S., Pomeroy, J. W., Pietroniro, A., & Cannon, A. (2020). High-resolution meteorological forcing data for hydrological modelling and climate change impact analysis in the Mackenzie River basin. *Earth System Science Data*, *12*(1), 629–645. https://doi.org/10.5194/essd-12-629-2020

Asong, Z. E., Wheater, H., Pomeroy, J., Pietroniro, A., Elshamy, M., Princz, D., & Cannon, A. (2022). High-resolution meteorological forcing data for hydrological modelling and climate change impact analysis over most of North America, 1951–2100. https://doi.org/10.20383/103.0622

Aubry-Wake, C., Bertoncini, A., & Pomeroy, J. W. (2022). Fire and ice: The impact of wildfire-affected albedo and irradiance on Glacier melt. *Earth's Future*, *10*(4), e2022EF002685. https://doi.org/10.1029/2022EF002685

Aubry-Wake, C., & Pomeroy, J. W. (2023). Predicting hydrological change in an alpine glacierized basin and its sensitivity to landscape evolution and meteorological forcings. *Water Resources Research*, *59*(9), e2022WR033363. https://doi.org/10.1029/2022WR033363

Baltzer, J. L., Veness, T., Chasmer, L. E., Sniderhan, A. E., & Quinton, W. L. (2014). Forests on thawing permafrost: Fragmentation, edge effects, and net forest loss. *Global Change Biology*, *20*(3), 824–834. https://doi.org/10.1111/GCB.12349

Beilman, D. W., & Robinson, S. D. (2003). Peatland permafrost thaw and landform type along a climatic gradient. In *Proceedings of the 8th International Conference on Permafrost*.

Berg, E. E., David Henry, J., Fastie, C. L., De Volder, A. D., & Matsuoka, S. M. (2006). Spruce beetle outbreaks on the Kenai Peninsula, Alaska, and Kluane national park and reserve, Yukon Territory: Relationship to summer temperatures and regional differences in disturbance regimes. *Forest Ecology and Management*, *227*(3), 219–232. https://doi.org/10.1016/J.FORECO.2006.02.038

Best, M. J., Pryor, M., Clark, D. B., Rooney, G. G., Essery, R. L. H., Ménard, C. B., et al. (2011). The Joint UK Land Environment Simulator (JULES), model description-Part 1: Energy and water fluxes. *Geoscientific Model Development*, *4*(3), 677–699. https://doi.org/10.5194/gmd-4-677-2011

Betts, A. K., Ball, J. H., Beljaars, A. C. M., Miller, M. J., & Viterbo, P. A. (1996). The land surface-atmosphere interaction: A review based on observational and global modeling perspectives. *Journal of Geophysical Research*, *101*(D3), 7209–7225. https://doi.org/10.1029/95JD02135

Boluwade, A., Zhao, K.-Y., Stadnyk, T. A., & Rasmussen, P. (2018). Towards validation of the Canadian Precipitation Analysis (CaPA) for hydrologic modeling applications in the Canadian Prairies. *Journal of Hydrology*, *556*, 1244–1255. https://doi.org/10.1016/j.jhydrol.2017.05.059

Brown, J., Ferrians, O., Heginbottom, J. A., & Melnikov, E. (2002). Circum-Arctic map of permafrost and ground-ice conditions, version 2. *National Snow and Ice Data Center (NSIDC)*. https://catalogue.ceda.ac.uk/uuid/b25d4a6174de4ac78000d034f500a268

Burke, E. J., Zhang, Y., & Krinner, G. (2020). Evaluating permafrost physics in the Coupled Model Intercomparison Project 6 (CMIP6) models and their sensitivity to climate change. *The Cryosphere*, *14*(9), 3155–3174. https://doi.org/10.5194/tc-14-3155-2020

Burn, D. H. (2008). Climatic influences on streamflow timing in the headwaters of the Mackenzie River basin. *Journal of Hydrology*, *352*(1–2), 225–238. https://doi.org/10.1016/J.JHYDROL.2008.01.019

Busschaert, L., De Roos, S., Thiery, W., Raes, D., & De Lannoy, G. J. M. (2022). Net irrigation requirement under different climate scenarios using AquaCrop over Europe. *Hydrology and Earth System Sciences*, *26*(14), 3731–3752. https://doi.org/10.5194/hess-26-3731-2022

Canada Centre for Remote Sensing (CCRS), Nacional para el Conocimiento y Uso de la Biodiversidad (CONABIO), Comisión Nacional Forestal (CONAFOR), Insituto Nacional de Estadística y Geografía (INEGIU.S. Geological Survey (USGS)). (2010). 2005 north American land cover at 250 m spatial resolution. *Canada Centre for Remote Sensing (CCRS), U.S. Geological Survey, INEGI, Commission for Environmental Cooperation*. Retrieved from http://www.cec.org/tools-and-resources/map-files/land-cover-2005

Cannon, A. J. (2018). Multivariate quantile mapping bias correction: An N-dimensional probability density function transform for climate model simulations of multiple variables. *Climate Dynamics*, *50*(1–2), 31–49. https://doi.org/10.1007/s00382-017-3580-6

Carey, S. K., Quinton, W. L., & Goeller, N. T. (2007). Field and laboratory estimates of pore size properties and hydraulic characteristics for subarctic organic soils. *Hydrological Processes*, *21*(19), 2560–2571. https://doi.org/10.1002/hyp.6795

Carmack, E. C., Yamamoto-Kawai, M., Haine, T. W. N., Bacon, S., Bluhm, B. A., Lique, C., et al. (2016). Freshwater and its role in the Arctic Marine system: Sources, disposition, storage, export, and physical and biogeochemical consequences in the Arctic and global oceans. *Journal of Geophysical Research: Biogeosciences*, *121*(3), 675–717. https://doi.org/10.1002/2015JG003140

Centre for Land and Biological Resources Research. (1996). *Soil landscape of Canada version 2.2. research branch*. Agriculture and Agri-Food Canada. Ottawa Retrieved from http://sis.agr.gc.ca/cansis/nsdb/slc/v2.2/index.html

Chadburn, S. E., Burke, E. J., Cox, P. M., Friedlingstein, P., Hugelius, G., & Westermann, S. (2017). An observation-based constraint on permafrost loss as a function of global warming. *Nature Climate Change*, *7*(5), 340–344. https://doi.org/10.1038/nclimate3262

Chen, Y. (2023). SWOT's eyes over Earth's surface water. *Nature Water*, *1*(2), 129–130. https://doi.org/10.1038/s44221-023-00029-0

Clark, D. B., Mercado, L. M., Sitch, S., Jones, C. D., Gedney, N., Best, M. J., et al. (2011). The Joint UK Land Environment Simulator (JULES), model description – Part 2: Carbon fluxes and vegetation dynamics. *Geoscientific Model Development*, *4*(3), 701–722. https://doi.org/10.5194/GMD-4-701-2011

Clarke, G. K. C., Jarosch, A. H., Anslow, F. S., Radić, V., & Menounos, B. (2015). Projected deglaciation of western Canada in the twenty-first century. *Nature Geoscience*, *8*(5), 372–377. https://doi.org/10.1038/ngeo2407

Cohen, S. J. (1997). What if and so what in northwest Canada: Could climate change make a difference to the future of the Mackenzie basin? *Arctic*, *50*(4), 4. https://doi.org/10.14430/arctic1112

Connon, R. F., Quinton, W. L., Craig, J. R., & Hayashi, M. (2014). Changing hydrologic connectivity due to permafrost thaw in the lower Liard River valley, NWT, Canada. *Hydrological Processes*, *28*(14), 4163–4178. https://doi.org/10.1002/hyp.10206

Côté, J., Desmarais, J.-G., Gravel, S., Méthot, A., Patoine, A., Staniforth, A., & Roch, M. (1998a). The operational CMC – MRB Global Environmental Multiscale (GEM) model. Part II: Results. *Monthly Weather Review*, *126*(6), 1397–1418. https://doi.org/10.1175/1520-0493(1998)126<1397:TOCMGE>2.0.CO;2

Côté, J., Gravel, S., Méthot, A., Patoine, A., Roch, M., Staniforth, A., et al. (1998b). The operational CMC-MRB Global Environmental Multiscale (GEM) model. Part I: Design considerations and formulation. *Monthly Weather Review*, *126*(6), 1373–1395. https://doi.org/10.1175/1520-0493(1998)126%3C1373:TOCMGE%3E2.0.CO;2

DeBeer, C. M., Sharp, M., & Schuster-Wallace, C. (2020). Glaciers and ice sheets. In *Encyclopedia of the world's biomes: Volumes 1–5* (Vol. 1–5, pp. V4-182–V4-194). https://doi.org/10.1016/B978-0-12-409548-9.12441-8

DeBeer, C. M., Wheater, H. S., Carey, S. K., & Chun, K. P. (2016). Recent climatic, cryospheric, and hydrological changes over the interior of western Canada: A review and synthesis. *Hydrology and Earth System Sciences*, *20*(4), 1573–1598. https://doi.org/10.5194/hess-20-1573-2016

DeBeer, C. M., Wheater, H. S., Pomeroy, J. W., Barr, A. G., Baltzer, J. L., Johnstone, J. F., et al. (2021). Summary and synthesis of Changing Cold Regions Network (CCRN) research in the interior of western Canada—Part 2: Future change in cryosphere, vegetation, and hydrology. *Hydrology and Earth System Sciences*, *25*(4), 1849–1882. https://doi.org/10.5194/hess-25-1849-2021

Derksen, C., Burgess, D., Duguay, C., Howell, S., Mudryk, L., Smith, S., et al. (2019). Changes in snow, ice, and permafrost across Canada. In *Canada's changing climate report* (pp. 194–260).

Deser, C., Knutti, R., Solomon, S., & Phillips, A. S. (2012). Communication of the role of natural variability in future North American climate. *Nature Climate Change*, *2*(11), 775–779. https://doi.org/10.1038/nclimate1562

Dupont, F., Chittibabu, P., Fortin, V., Rao, Y. R., & Lu, Y. (2012). Assessment of a NEMO-based hydrodynamic modelling system for the Great Lakes. *Water Quality Research Journal*, *47*(3–4), 198–214. https://doi.org/10.2166/wqrjc.2012.014

19447973, 2025, 12, Downloaded from https://agupubs.onlinelibrary.wiley.com/doi/10.1029/2024WR039276 by University Of Saskatchewan, Wiley Online Library on [08/12/2025]. See the Terms and Conditions (https://onlinelibrary.wiley.com/terms-and-conditions) on Wiley Online Library for rules of use; OA articles are governed by the applicable Creative Commons License

Elshamy, M. E., Pomeroy, J. W., Pietroniro, A., Wheater, H., Abdelhamed, M., & Davison, B. (2025). Land surface hydrological modelling of the Mackenzie River basin: Parametrization to simulate streamflow and permafrost dynamics. *Journal of Hydrology*, *659*, 133134. https://doi.org/10.1016/j.jhydrol.2025.133134

Elshamy, M. E., Princz, D., Sapriza-Azuri, G., Abdelhamed, M. S., Pietroniro, A., Wheater, H. S., & Razavi, S. (2020). On the configuration and initialization of a large-scale hydrological land surface model to represent permafrost. *Hydrology and Earth System Sciences*, *24*(1), 349–379. https://doi.org/10.5194/hess-24-349-2020

Farquharson, L. M., Romanovsky, V. E., Cable, W. L., Walker, D. A., Kokelj, S. V., & Nicolsky, D. (2019). Climate change drives widespread and rapid thermokarst development in very cold permafrost in the Canadian High Arctic. *Geophysical Research Letters*, *46*(12), 6681–6689. https://doi.org/10.1029/2019GL082187

Ford, J. D., Couture, N., Bell, T., & Clark, D. G. (2018). Climate change and Canada's north coast: Research trends, progress, and future directions. *Environmental Reviews*, *26*(1), 82–92. https://doi.org/10.1139/er-2017-0027

Fortin, V., Roy, G., Stadnyk, T., Koenig, K., Gasset, N., & Mahidjiba, A. (2018). Ten years of science based on the Canadian Precipitation Analysis: A CaPA system overview and literature review. *Atmosphere-Ocean*, *56*(3), 178–196. https://doi.org/10.1080/07055900.2018.1474728

Gao, C., Booij, M. J., & Xu, Y.-P. (2020). Assessment of extreme flows and uncertainty under climate change: Disentangling the uncertainty contribution of representative concentration pathways, global climate models and internal climate variability. *Hydrology and Earth System Sciences*, *24*(6), 3251–3269. https://doi.org/10.5194/hess-24-3251-2020

Garnaud, C., MacKay, M., & Fortin, V. (2022). A one-dimensional Lake model in ECCC's land surface prediction system. *Journal of Advances in Modeling Earth Systems*, *14*(2), e2021MS002861. https://doi.org/10.1029/2021MS002861

Gelfan, A., Gustafsson, D., Motovilov, Y., Arheimer, B., Kalugin, A., Krylenko, I., et al. (2017). Climate change impact on the water regime of two great Arctic Rivers: Modeling and uncertainty issues. *Climatic Change*, *141*(3), 499–515. https://doi.org/10.1007/s10584-016-1710-5

Giorgi, F., Jones, C., & Asrar, G. R. (2009). Addressing climate information needs at the regional level: The CORDEX framework. https://www.researchgate.net/publication/265311339_Addressing_climate_information_needs_at_the_regional_level_The_CORDEX_framework

Gosling, S. N., Taylor, R. G., Arnell, N. W., & Todd, M. C. (2011). A comparative analysis of projected impacts of climate change on river runoff from global and catchment-scale hydrological models. *Hydrology and Earth System Sciences*, *15*(1), 279–294. https://doi.org/10.5194/HESS-15-279-2011

Gruber, S. (2012). Derivation and analysis of a high-resolution estimate of global permafrost zonation. *The Cryosphere*, *6*(1), 221–233. https://doi.org/10.5194/TC-6-221-2012

Hanes, C. C., Wang, X., Jain, P., Parisien, M. A., Little, J. M., & Flannigan, M. D. (2019). Fire-regime changes in Canada over the last half century. *Canadian Journal of Forest Research*, *49*(3), 256–269. https://doi.org/10.1139/CJFR-2018-0293/SUPPL_FILE/CJFR-2018-0293SUPPLA.DOCX

Hannah, L., Roehrdanz, P. R., Bahadur, K., Id, K. C., Fraser, E. D. G., Donatti, C. I., et al. (2020). The environmental consequences of climate-driven agricultural frontiers. *15*(2), e0228305. https://doi.org/10.1371/journal.pone.0228305

Harris, C., Arenson, L. U., Christiansen, H. H., Etzelmüller, B., Frauenfelder, R., Gruber, S., et al. (2009). Permafrost and climate in Europe: Monitoring and modelling thermal, geomorphological and geotechnical responses. *Earth-Science Reviews*, *92*(3–4), 117–171. https://doi.org/10.1016/J.EARSCIREV.2008.12.002

Husain, S. Z., Alavi, N., Bélair, S., Carrera, M., Zhang, S., Fortin, V., et al. (2016). The multibudget Soil, Vegetation, and Snow (SVS) scheme for land surface parameterization: Offline warm season evaluation. *Journal of Hydrometeorology*, *17*(8), 2293–2313. https://doi.org/10.1175/JHM-D-15-0228.1

Jacques, J. M. S., & Sauchyn, D. J. (2009). Increasing winter baseflow and mean annual streamflow from possible permafrost thawing in the Northwest Territories, Canada. *Geophysical Research Letters*, *36*(1). https://doi.org/10.1029/2008GL035822

Jansson, J. K., & Hofmockel, K. S. (2020). Soil microbiomes and climate change. *Nature Reviews Microbiology 2019*, *18*(1), 35–46. https://doi.org/10.1038/s41579-019-0265-7

Ji, H., Nan, Z., Hu, J., Zhao, Y., & Zhang, Y. (2022). On the Spin-Up strategy for spatial modeling of permafrost dynamics: A case study on the Qinghai-Tibet Plateau. *Journal of Advances in Modeling Earth Systems*, *14*(3), e2021MS002750. https://doi.org/10.1029/2021MS002750

Jin, K., Jin, Y., Wang, F., & Zong, Q. (2023). Should time-lag and time-accumulation effects of climate be considered in attribution of vegetation dynamics? Case study of China's temperate grassland region. *International Journal of Biometeorology*, *67*(7), 1213–1223. https://doi.org/10.1007/s00484-023-02489-1

Johnstone, J. F., Chapin, F. S., Hollingsworth, T. N., Mack, M. C., Romanovsky, V., & Turetsky, M. (2010). Fire, climate change, and forest resilience in interior Alaska1. *Canadian Journal of Forest Research*, *40*(7), 1302–1312. https://doi.org/10.1139/X10-061/ASSET/IMAGES/LARGE/X10-061F6.JPEG

Kouwen, N. (1988). WATFLOOD: A micro-computer based flood forecasting system based on real-time weather Radar. *Canadian Water Resources Journal*, *13*(1), 62–77. https://doi.org/10.4296/cwrj1301062

Kouwen, N., Soulis, E. D., Pietroniro, A., Donald, J., & Harrington, R. A. (1993). Grouped response units for distributed hydrologic modeling. *Journal of Water Resources Planning and Management*, *119*(3), 289–305. https://doi.org/10.1061/(asce)0733-9496(1993)119:3(289)

Koven, C. D., Riley, W. J., & Stern, A. (2013). Analysis of permafrost thermal dynamics and response to climate change in the CMIP5 Earth system models. *Journal of Climate*, *26*(6), 1877–1900. https://doi.org/10.1175/JCLI-D-12-00228.1

Krogh, S. A., & Pomeroy, J. W. (2021). Simulating site-scale permafrost hydrology: Sensitivity to modelling decisions and air temperature. *Journal of Hydrology*, *602*, 126771. https://doi.org/10.1016/j.jhydrol.2021.126771

Lamontagne-Hallé, P., McKenzie, J. M., Kurylyk, B. L., Molson, J., & Lyon, L. N. (2020). Guidelines for cold-regions groundwater numerical modeling. *Wiley Interdisciplinary Reviews: Water*, (June), 1–26. https://doi.org/10.1002/wat2.1467

Lange, S. (2019). Trend-preserving bias adjustment and statistical downscaling with ISIMIP3BASD (v1.0). *Geoscientific Model Development*, *12*(7), 3055–3070. https://doi.org/10.5194/gmd-12-3055-2019

Lawrence, D. M., & Slater, A. G. (2008). Incorporating organic soil into a global climate model. *Climate Dynamics*, *30*(2–3), 145–160. https://doi.org/10.1007/s00382-007-0278-1

Lawrence, D. M., Slater, A. G., Romanovsky, V. E., & Nicolsky, D. J. (2008). Sensitivity of a model projection of near-surface permafrost degradation to soil column depth and representation of soil organic matter. *Journal of Geophysical Research*, *113*(2), 1–14. https://doi.org/10.1029/2007JF000883

Leduc, M., Mailhot, A., Frigon, A., Martel, J.-L., Ludwig, R., Brietzke, G. B., et al. (2019). The ClimEx project: A 50-Member ensemble of climate change projections at 12-km resolution over Europe and northeastern North America with the Canadian Regional Climate Model (CRCM5). *Journal of Applied Meteorology and Climatology*, *58*(4), 663–693. https://doi.org/10.1175/JAMC-D-18-0021.1

19447973, 2025, 12, Downloaded from https://agupubs.onlinelibrary.wiley.com/doi/10.1029/2024WR039276 by University Of Saskatchewan, Wiley Online Library on [08/12/2025]. See the Terms and Conditions (https://onlinelibrary.wiley.com/terms-and-conditions) on Wiley Online Library for rules of use; OA articles are governed by the applicable Creative Commons License

Liu, W., Yang, T., Sun, F., Wang, H., Feng, Y., & Du, M. (2021). Observation-constrained projection of global flood magnitudes with anthropogenic warming. *Water Resources Research*, *57*(3), e2020WR028830. https://doi.org/10.1029/2020WR028830
Louie, P. Y. T., Hogg, W. D., MacKay, M. D., Zhang, X., & Hopkinson, R. F. (2002). The water balance climatology of the Mackenzie basin with reference to the 1994/95 water year. *Atmosphere-Ocean*, *40*(2), 159–180. https://doi.org/10.3137/ao.400206
Luo, Y., Arnold, J., Allen, P., & Chen, X. (2012). Baseflow simulation using SWAT model in an inland river basin in Tianshan Mountains, Northwest China. *Hydrology and Earth System Sciences*, *16*(4), 1259–1267. https://doi.org/10.5194/hess-16-1259-2012
Mahfouf, J.-F. F., Brasnett, B., & Gagnon, S. (2007). A Canadian Precipitation Analysis (CaPA) project: Description and preliminary results. *Atmosphere-Ocean*, *45*(1), 1–17. https://doi.org/10.3137/ao.v450101
Mai, J., Tolson, B. A., Shen, H., Gaborit, É., Fortin, V., Gasset, N., et al. (2021). Great Lakes Runoff Intercomparison Project phase 3: Lake Erie (GRIP-E). *Journal of Hydrologic Engineering*, *26*(9), 05021020. https://doi.org/10.1061/(ASCE)HE.1943-5584.0002097
McGuire, A. D., Lawrence, D. M., Koven, C., Clein, J. S., Burke, E., Chen, G., et al. (2018). Dependence of the evolution of carbon dynamics in the northern permafrost region on the trajectory of climate change. *Proceedings of the National Academy of Sciences of the United States of America*, *115*(15), 3882–3887. https://doi.org/10.1073/pnas.1719903115
McPhee, M. G., Proshutinsky, A., Morison, J. H., Steele, M., & Alkire, M. B. (2009). Rapid change in freshwater content of the Arctic Ocean. *Geophysical Research Letters*, *36*(10). https://doi.org/10.1029/2009GL037525
Melton, J. R., & Arora, V. K. (2016). Competition between plant functional types in the Canadian Terrestrial Ecosystem Model (CTEM) v. 2.0. *Geoscientific Model Development*, *9*(1), 323–361. https://doi.org/10.5194/GMD-9-323-2016
Melton, J. R., Arora, V. K., Wisernig-Cojoc, E., Seiler, C., Fortier, M., Chan, E., & Teckentrup, L. (2020). CLASSIC v1.0: The open-source community successor to the Canadian Land Surface Scheme (CLASS) and the Canadian Terrestrial Ecosystem Model (CTEM) – Part 1: Model framework and site-level performance. *Geoscientific Model Development*, *13*(6), 1–40. https://doi.org/10.5194/gmd-13-2825-2020
Meyer, G., Humphreys, E. R., Melton, J. R., Cannon, A. J., & Lafleur, P. M. (2021). Simulating shrubs and their energy and carbon dioxide fluxes in Canada's Low Arctic with the Canadian Land Surface Scheme including Biogeochemical Cycles (CLASSIC). *Biogeosciences*, *18*(11), 3263–3283. https://doi.org/10.5194/bg-18-3263-2021
Morse, P. D., Wolfe, S. A., Kokelj, S. V., & Gaanderse, A. J. R. (2016). The occurrence and thermal disequilibrium state of permafrost in forest ecotopes of the great slave region, Northwest Territories, Canada. *Permafrost and Periglacial Processes*, *27*(2), 145–162. https://doi.org/10.1002/PPP.1858
Natural Resources Canada. (2006). The atlas of Canada. *Natural Resources Canada*. Retrieved from https://natural-resources.canada.ca/maps-tools-and-publications/maps/atlas-canada/10784
Natural Resources Canada. (2013). Canadian digital elevation model product specifications—edition 1.1 [Dataset]. Retrieved from https://canwinmap.ad.umanitoba.ca/documents/246
Obu, J., Westermann, S., Bartsch, A., Berdnikov, N., Christiansen, H. H., Dashtseren, A., et al. (2019). Northern Hemisphere permafrost map based on TTOP modelling for 2000–2016 at 1 km_2 scale. *Earth-Science Reviews*, *193*, 299–316. https://doi.org/10.1016/j.earscirev.2019.04.023
O'Neill, H. B., Burn, C. R., Allard, M., Arenson, L. U., Bunn, M. I., Connon, R. F., et al. (2020). Permafrost thaw and northern development. *Nature Climate Change*, *10*(8), 722–723. https://doi.org/10.1038/s41558-020-0862-5
Paquin, D., Giguère, M., McCray, C., Asselin, O., Gauthier, C., Matte, D., et al. (2024). CRCM5-CMIP6: A dynamically-downscaled ensemble of CMIP6 simulations [Dataset]. *Zenodo*. https://doi.org/10.5281/zenodo.11122934
Pastick, N. J., Jorgenson, M. T., Wylie, B. K., Rose, J. R., Rigge, M., & Walvoord, M. A. (2014). Spatial variability and landscape controls of near-surface permafrost within the Alaskan Yukon River basin. *Journal of Geophysical Research: Biogeosciences*, *119*(6), 1244–1265. https://doi.org/10.1002/2013JG002594
Pietroniro, A., Fortin, V., Kouwen, N., Neal, C., Turcotte, R., Davison, B., et al. (2007). Development of the MESH modelling system for hydrological ensemble forecasting of the Laurentian Great Lakes at the regional scale. *Hydrology and Earth System Sciences*, *11*(4), 1279–1294. https://doi.org/10.5194/hess-11-1279-2007
Pietroniro, A., & Soulis, E. D. (2003). A hydrology modelling framework for the Mackenzie GEWEX programme. *Hydrological Processes*, *17*(3), 673–676. https://doi.org/10.1002/hyp.5104
Pomeroy, J. W., Gray, D. M., & Marsh, P. (2008). Studies on snow redistribution by wind and forest, snow-covered area depletion, and frozen soil infiltration in Northern and Western Canada. *Cold Region Atmospheric and Hydrologic Studies. The Mackenzie GEWEX Experience*, *2*, 81–96. https://doi.org/10.1007/978-3-540-75136-6_5
Pradhananga, D., & Pomeroy, J. W. (2022). Diagnosing changes in glacier hydrology from physical principles using a hydrological model with snow redistribution, sublimation, firnification and energy balance ablation algorithms. *Journal of Hydrology*, *608*, 127545. https://doi.org/10.1016/j.jhydrol.2022.127545
Prentice, C. (1992). Climate and long term vegetation dynamics. In *Plant succession: Theory and prediction* (1st ed., pp. 293–339). Chapman & Hall.
Quante, L., Willner, S. N., Middelanis, R., & Levermann, A. (2021). Regions of intensification of extreme snowfall under future warming. *Scientific Reports 2021*, *11*(1), 1–9. https://doi.org/10.1038/s41598-021-95979-4
Quinton, W. L., Berg, A., Braverman, M., Carpino, O., Chasmer, L., Connon, R., et al. (2019). A synthesis of three decades of hydrological research at scotty creek, NWT, Canada. *Hydrology and Earth System Sciences*, *23*(4), 2015–2039. https://doi.org/10.5194/HESS-23-2015-2019
Quinton, W. L., Hayashi, M., & Chasmer, L. E. (2011). Permafrost-thaw-induced land-cover change in the Canadian subarctic: Implications for water resources. *Hydrological Processes*, *25*(1), 152–158. https://doi.org/10.1002/hyp.7894
Rajulapati, C. R., Gaddam, R. K., Nerantzaki, S. D., Papalexiou, S. M., Cannon, A. J., & Clark, M. P. (2022). Exacerbated heat in large Canadian cities. *Urban Climate*, *42*, 101097. https://doi.org/10.1016/J.UCLIM.2022.101097
Ran, Y., Li, X., Cheng, G., Che, J., Aalto, J., Karjalainen, O., et al. (2022). New high-resolution estimates of the permafrost thermal state and hydrothermal conditions over the Northern Hemisphere. *Earth System Science Data*, *14*(2), 865–884. https://doi.org/10.5194/essd-14-865-2022
Rasouli, K., Pomeroy, J. W., & Whitfield, P. H. (2019). Are the effects of vegetation and soil changes as important as climate change impacts on hydrological processes? *Hydrology and Earth System Sciences*, *23*(12), 4933–4954. https://doi.org/10.5194/hess-23-4933-2019
Rehfeldt, G. E., Crookston, N. L., Sáenz-Romero, C., & Campbell, E. M. (2012). North American vegetation model for land-use planning in a changing climate: A solution to large classification problems. *Ecological Applications*, *22*(1), 119–141. https://doi.org/10.1890/11-0495.1
RGI Consortium. (2017). Randolph glacier inventory—A dataset of global glacier outlines, version 6 [Dataset]. *National Snow and Ice Data Center*. https://doi.org/10.7265/N5-RGI-60

19447973, 2025, 12, Downloaded from https://agupubs.onlinelibrary.wiley.com/doi/10.1029/2024WR039276 by University Of Saskatchewan, Wiley Online Library on [08/12/2025]. See the Terms and Conditions (https://onlinelibrary.wiley.com/terms-and-conditions) on Wiley Online Library for rules of use; OA articles are governed by the applicable Creative Commons License

Riseborough, D., Shiklomanov, N., Etzelmuller, B., Gruber, S., Marchenko, S., Johansson, M., et al. (2008). Recent advances in permafrost modelling. *Permafrost and Periglacial Processes*, *19*(2), 137–156. https://doi.org/10.1002/ppp.615

Roelfsema, M., van Soest, H. L., Harmsen, M., van Vuuren, D. P., Bertram, C., den Elzen, M., et al. (2020). Taking stock of national climate policies to evaluate implementation of the Paris agreement. *Nature Communications*, *11*(1), 2096. https://doi.org/10.1038/s41467-020-15414-6

Rokaya, P., Peters, D. L., Bonsal, B., Wheater, H., & Lindenschmidt, K. (2019a). Modelling the effects of climate and flow regulation on ice-affected backwater staging in a large northern river. *River Research and Applications*, *35*(6), 587–600. https://doi.org/10.1002/rra.3436

Rokaya, P., Peters, D. L., Elshamy, M. E., Budhathoki, S., & Lindenschmidt, K. E. (2019b). Impacts of future climate on the hydrology of a northern headwaters basin and its implications for a downstream deltaic ecosystem. *Hydrological Processes*, *34*(7), 1–17. https://doi.org/10.1002/hyp.13687

Romanovsky, V. E., Smith, S. L., & Christiansen, H. H. (2010). Permafrost thermal state in the polar northern Hemisphere during the international polar year 2007–2009: A synthesis. *Permafrost and Periglacial Processes*, *21*(2), 106–116. https://doi.org/10.1002/ppp.689

Rood, S. B., Kaluthota, S., Philipsen, L. J., Rood, N. J., & Zanewich, K. P. (2017). Increasing discharge from the Mackenzie River system to the Arctic Ocean. *Hydrological Processes*, *31*(1), 150–160. https://doi.org/10.1002/HYP.10986

Rounce, D. R., Hock, R., Maussion, F., Hugonnet, R., Kochtitzky, W., Huss, M., et al. (2023). Global glacier change in the 21st century: Every increase in temperature matters. *Science*, *379*(6), 78–83. https://doi.org/10.1126/science.abo1324

Schellnhuber, H. J., Rahmstorf, S., & Winkelmann, R. (2016). Why the right climate target was agreed in Paris. *Nature Climate Change 2016*, *6*(7), 649–653. https://doi.org/10.1038/nclimate3013

Schlund, M., Lauer, A., Gentine, P., Sherwood, S. C., & Eyring, V. (2020). Emergent constraints on equilibrium climate sensitivity in CMIP5: Do they hold for CMIP6? *Earth System Dynamics*, *11*(4), 1233–1258. https://doi.org/10.5194/esd-11-1233-2020

Schuur, E. A. G., McGuire, A. D., Schädel, C., Grosse, G., Harden, J. W., Hayes, D. J., et al. (2015). Climate change and the permafrost carbon feedback. *Nature*, *520*(7546), 171–179. https://doi.org/10.1038/nature14338

Schwalm, C. R., Glendon, S., & Duffy, P. B. (2020). RCP8.5 tracks cumulative CO_2 emissions. *Proceedings of the National Academy of Sciences*, *117*(33), 19656–19657. https://doi.org/10.1073/pnas.2007117117

Scinocca, J. F., Kharin, V. V., Jiao, Y., Qian, M. W., Lazare, M., Solheim, L., et al. (2016). Coordinated global and regional climate modeling. *Journal of Climate*, *29*(1), 17–35. https://doi.org/10.1175/JCLI-D-15-0161.1

Shangguan, W., Hengl, T., Mendes de Jesus, J., Yuan, H., & Dai, Y. (2017). Mapping the global depth to bedrock for land surface modeling. *Journal of Advances in Modeling Earth Systems*, *9*(1), 65–88. https://doi.org/10.1002/2016MS000686

Shannon, S., Smith, R., Wiltshire, A., Payne, T., Huss, M., Betts, R., et al. (2019). Global glacier volume projections under high-end climate change scenarios. *The Cryosphere*, *13*(1), 325–350. https://doi.org/10.5194/tc-13-325-2019

Sheffield, J., Barrett, A. P., Colle, B., Fernando, D. N., Fu, R., Geil, K. L., et al. (2013a). North American climate in CMIP5 experiments. Part I: Evaluation of historical simulations of continental and regional climatology. *Journal of Climate*, *26*(23), 9209–9245. https://doi.org/10.1175/JCLI-D-12-00592.1

Sheffield, J., Camargo, S. J., Fu, R., Hu, Q., Jiang, X., Johnson, N., et al. (2013b). North American climate in CMIP5 experiments. Part II: Evaluation of historical simulations of intraseasonal to decadal variability. *Journal of Climate*, *26*(23), 9247–9290. https://doi.org/10.1175/JCLI-D-12-00593.1

Shrestha, R. R., Cannon, A. J., Schnorbus, M. A., & Alford, H. (2019). Climatic controls on future hydrologic changes in a subarctic River basin in Canada. *Journal of Hydrometeorology*, *20*(9), 1757–1778. https://doi.org/10.1175/JHM-D-18-0262.1

Shur, Y. L., & Jorgenson, M. T. (2007). Patterns of permafrost formation and degradation in relation to climate and ecosystems. *Permafrost and Periglacial Processes*, *18*(1), 7–19. https://doi.org/10.1002/PPP.582

Smith, S. L., Throop, J., & Lewkowicz, A. G. (2012). Recent changes in climate and permafrost temperatures at forested and polar desert sites in Northern Canada. *Canadian Journal of Earth Sciences*, *49*(8), 914–924. https://doi.org/10.1139/E2012-019

Soulis, E. D., & Seglenieks, F. R. (2008). The MAGS integrated modeling system. *Cold Region Atmospheric and Hydrologic Studies. The Mackenzie GEWEX Experience*, *2*, 445–473. https://doi.org/10.1007/978-3-540-75136-6_24

Soulis, E. D., Snelgrove, K. R., Kouwen, N., Seglenieks, F., & Verseghy, D. L. (2000). Towards closing the vertical water balance in Canadian atmospheric models: Coupling of the land surface scheme class with the distributed hydrological model watflood. *Atmosphere-Ocean*, *38*(1), 251–269. https://doi.org/10.1080/07055900.2000.9649648

Stewart, R. E., Leighton, H. G., Marsh, P., Moore, G. W. K., Ritchie, H., Rouse, W. R., et al. (1998). The Mackenzie GEWEX study: The water and energy cycles of a major North American River basin. *Bulletin of the American Meteorological Society*, *79*(12), 2665–2683. https://doi.org/10.1175/1520-0477(1998)079%3C2665:TMGSTW%3E2.0.CO;2

Strong, G. S., Proctor, B., Wang, M., Soulis, E. D., Smith, C. D., Seglenieks, F., & Snelgrove, K. (2002). Closing the Mackenzie basin water budget, water years 1994/95 to 1996/97. *Atmosphere-Ocean*, *40*(2), 113–124. https://doi.org/10.3137/ao.400203

Tapley, B. D., Bettadpur, S., Watkins, M., & Reigber, C. (2004). The gravity recovery and climate experiment: Mission overview and early results. *Geophysical Research Letters*, *31*(9). https://doi.org/10.1029/2004GL019920

Tesemma, Z., Pomeroy, J., Pietroniro, A., Davison, B., & Yassin, F. (n.d.). Improving Mountain hydrological predictions by better representing Mountain topography in hydrological land surface models. *SSRN Scholarly Paper No. 4737884*. (in review). https://doi.org/10.2139/ssrn.4737884

Teufel, B., & Sushama, L. (2019). Abrupt changes across the Arctic permafrost region endanger northern development. *Nature Climate Change 2019*, *9*(11), 858–862. https://doi.org/10.1038/s41558-019-0614-6

Thorne, R. (2011). Uncertainty in the impacts of projected climate change on the hydrology of a subarctic environment: Liard River basin. *Hydrology and Earth System Sciences*, *15*(5), 1483–1492. https://doi.org/10.5194/HESS-15-1483-2011

Tittensor, D. P., Novaglio, C., Harrison, C. S., Heneghan, R. F., Barrier, N., Bianchi, D., et al. (2021). Next-generation ensemble projections reveal higher climate risks for marine ecosystems. *Nature Climate Change 2021*, *11*(11), 973–981. https://doi.org/10.1038/s41558-021-01173-9

Turetsky, M. R., Baltzer, J. L., Johnstone, J. F., Mack, M. C., McCann, K., & Schuur, E. A. G. (2017). Losing legacies, ecological release, and transient responses: Key challenges for the future of northern ecosystem science. *Ecosystems*, *20*(1), 23–30. https://doi.org/10.1007/S10021-016-0055-2/FIGURES/1

Vanderkelen, I., Gharari, S., Mizukami, N., Clark, M. P., Lawrence, D. M., Swenson, S., et al. (2022). Evaluating a reservoir parametrization in the vector-based global routing model mizuRoute (v2.0.1) for Earth system model coupling. *Geoscientific Model Development*, *15*(10), 4163–4192. https://doi.org/10.5194/gmd-15-4163-2022

van Everdingen, R. O. (2005). Glossary of permafrost and related ground-ice terms. In *Multi-language glossary of permafrost and related ground ice terms*. International Permafrost Association. https://doi.org/10.2307/1551636.213

Verseghy, D. L. (1991). Class—A Canadian land surface scheme for GCMS. I. Soil model. *International Journal of Climatology*, *11*(2), 111–133. https://doi.org/10.1002/joc.3370110202

19447973, 2025, 12, Downloaded from https://agupubs.onlinelibrary.wiley.com/doi/10.1029/2024WR039276 by University Of Saskatchewan, Wiley Online Library on [08/12/2025]. See the Terms and Conditions (https://onlinelibrary.wiley.com/terms-and-conditions) on Wiley Online Library for rules of use; OA articles are governed by the applicable Creative Commons License

Verseghy, D. L. (2012). CLASS – The Canadian land surface scheme (version 3.6)—Technical documentation. *Internal Report, Climate Research Division, Science and Technology Branch, Environmental Canada*. https://www.canada.ca/en/environment-climate-change/services/climate-change/science-research-data/modeling-projections-analysis/canadian-land-surface-scheme.html

Verseghy, D. L., McFarlane, N. A., & Lazare, M. (1993). Class—A Canadian land surface scheme for GCMS, II. Vegetation model and coupled runs. *International Journal of Climatology*, *13*(4), 347–370. https://doi.org/10.1002/joc.3370130402

Vionnet, V., Mortimer, C., Brady, M., Arnal, L., & Brown, R. (2021). Canadian historical Snow Water Equivalent dataset (CanSWE, 1928–2020). *Earth System Science Data*, *13*(9), 4603–4619. https://doi.org/10.5194/essd-13-4603-2021

Walvoord, M. A., & Kurylyk, B. L. (2016). Hydrologic impacts of thawing permafrost—A review. *Vadose Zone Journal*, *15*(6), 1–20. https://doi.org/10.2136/vzj2016.01.0010

Weedon, G. P., Balsamo, G., Bellouin, N., Gomes, S., Best, M. J., & Viterbo, P. (2014). The WFDEI meteorological forcing dataset: WATCH forcing data methodology applied to ERA-interim reanalysis data. *Water Resources Research*, *50*, 7505–7514. https://doi.org/10.1002/2014WR015638.Received

Westermann, S., Duguay, C. R., Grosse, G., & Kääb, A. (2015). Remote sensing of permafrost and frozen ground. In M. Tedesco (Ed.), *Remote sensing of the cryosphere* (pp. 307–344). JohnWiley & Sons, Ltd. https://doi.org/10.1002/9781118368909.ch13

Wheater, H. S., Pomeroy, J. W., Pietroniro, A., Davison, B., Elshamy, M. E., Yassin, F., et al. (2022). Advances in modelling large river basins in cold regions with Modélisation Environmentale Communautaire—Surface and Hydrology (MESH), the Canadian hydrological land surface scheme. *Hydrological Processes*, *36*(4), e14557. https://doi.org/10.1002/hyp.14557

Wong, J. S., Razavi, S., Bonsal, B. R., Wheater, H. S., & Asong, Z. E. (2017). Inter-comparison of daily precipitation products for large-scale hydro-climatic applications over Canada. *Hydrology and Earth System Sciences*, *21*(4), 2163–2185. https://doi.org/10.5194/hess-21-2163-2017

Woo, M. (Ed.). (2008a). *Cold region atmospheric and hydrologic studies. The mackenzie GEWEX experience volume 1: Atmospheric dynamics*. Springer. https://doi.org/10.1007/978-3-540-73936-4

Woo, M. (Ed.). (2008b). *Cold region atmospheric and hydrologic studies. The mackenzie GEWEX experience volume 2: Htdrologic processes*. Springer. https://doi.org/10.1007/978-3-540-75136-6

Woo, M. (2012). *Permafrost hydrology*. Springer. https://doi.org/10.1007/978-3-642-23462-0

Woo, M., Lewkowicz, A. G., & Rouse, W. R. (1992). Response of the Canadian permafrost environment to climatic change. *Physical Geography*, *13*(4), 287–317. https://doi.org/10.1080/02723646.1992.10642459

Woo, M., & Marsh, P. (2005). Snow, frozen soils and permafrost hydrology in Canada, 1999–2002. *Hydrological Processes*, *19*(1), 215–229. https://doi.org/10.1002/hyp.5772

Woo, M., Mollinga, M., & Smith, S. L. (2007). Climate warming and active layer thaw in the boreal and tundra environments of the Mackenzie Valley. *Canadian Journal of Earth Sciences*, *44*(6), 733–743. https://doi.org/10.1139/E06-121

Yang, D., Shi, X., & Marsh, P. (2015). Variability and extreme of Mackenzie River daily discharge during 1973–2011. *Quaternary International*, *380*(381), 159–168. https://doi.org/10.1016/j.quaint.2014.09.023

Yassin, F., Razavi, S., Elshamy, M. E., Davison, B., Sapriza-Azuri, G., & Wheater, H. (2019). Representation of water management in hydrological and land surface models. *Hydrology and Earth System Sciences Discussions*, 1–35. https://doi.org/10.5194/hess-2019-7

Yassin, F., Razavi, S., Wheater, H., Sapriza-Azuri, G., Davison, B., & Pietroniro, A. (2017). Enhanced identification of a hydrologic model using streamflow and satellite water storage data: A multicriteria sensitivity analysis and optimization approach. *Hydrological Processes*, *31*(19), 3320–3333. https://doi.org/10.1002/hyp.11267

Yeh, K.-S., Côté, J., Gravel, S., Méthot, A., Patoine, A., Roch, M., et al. (2002). The CMC–MRB Global Environmental Multiscale (GEM) model. Part III: Nonhydrostatic formulation. *Monthly Weather Review*, *130*(2), 339–356. https://doi.org/10.1175/1520-0493(2002)130%3C0339:TCMGEM%3E2.0.CO;2

Yip, Q. K. Y., Burn, D. H., Seglenieks, F., Pietroniro, A., & Soulis, E. D. (2012). Climate impacts on hydrological variables in the Mackenzie River basin. *Canadian Water Resources Journal*, *37*(3), 209–230. https://doi.org/10.4296/cwrj2011-899

Yu, X., Millet, D. B., Henze, D. K., Turner, A. J., Delgado, A. L., Bloom, A. A., & Sheng, J. (2023). A high-resolution satellite-based map of global methane emissions reveals missing wetland, fossil fuel, and monsoon sources. *Atmospheric Chemistry and Physics*, *23*(5), 3325–3346. https://doi.org/10.5194/acp-23-3325-2023

Yun, X., Tang, Q., Sun, S., & Wang, J. (2021). Reducing climate change induced flood at the cost of hydropower in the Lancang-Mekong River basin. *Geophysical Research Letters*, *48*(20), e2021GL094243. https://doi.org/10.1029/2021GL094243

Zhang, F., Elshamy, M. E., & Lindenschmidt, K.-E. (2022). Climate change impacts on ice jam behavior in an inland Delta: A new ice jam projection framework. *Climatic Change*, *171*(1–2), 13. https://doi.org/10.1007/S10584-022-03312-3

Zhang, S., Gan, T. Y., Bush, A. B. G., & Zhang, G. (2023). Evaluation of the impact of climate change on the streamflow of major pan-Arctic river basins through machine learning models. *Journal of Hydrology*, *619*, 129295. https://doi.org/10.1016/J.JHYDROL.2023.129295

Zhang, X., Flato, G., Kirchmeier-Young, M., Vincent, L. A., Wan, H., Wang, X., et al. (2019). Changes in temperature and precipitation across Canada. In E. Bush & D. S. Lemmen (Eds.), *Canada's changing climate report* (pp. 112–193). Government of Canada.

Zhang, Y., Chen, W., & Riseborough, D. W. (2008). Disequilibrium response of permafrost thaw to climate warming in Canada over 1850–2100. *Geophysical Research Letters*, *35*(2), 2502. https://doi.org/10.1029/2007GL032117

Zhao, L., Wu, Q., Marchenko, S. S., & Sharkhuu, N. (2010). Thermal state of permafrost and active layer in central Asia during the international polar year. *Permafrost and Periglacial Processes*, *21*(2), 198–207. https://doi.org/10.1002/PPP.688

References From the Supporting Information

Hersbach, H., Bell, B., Berrisford, P., Hirahara, S., Horányi, A., Muñoz-Sabater, J., et al. (2020). The ERA5 global reanalysis. *Quarterly Journal of the Royal Meteorological Society*, *146*(730), 1999–2049. https://doi.org/10.1002/qj.3803

19447973, 2025, 12, Downloaded from https://agupubs.onlinelibrary.wiley.com/doi/10.1029/2024WR039276 by University Of Saskatchewan, Wiley Online Library on [08/12/2025]. See the Terms and Conditions (https://onlinelibrary.wiley.com/terms-and-conditions) on Wiley Online Library for rules of use; OA articles are governed by the applicable Creative Commons License